Journal of Manufacturing Processes 16 (2014) 4–25

Contents lists available at ScienceDirect

Journal of Manufacturing Processes

journal homepage: www.elsevier.com/locate/manpro

Technical paper

Welding processes for wear resistant overlays

Patricio F. Mendez [a,*], Nairn Barnes [a], Kurtis Bell [a,b], Steven D. Borle [a], Satya S. Gajapathi [c], Stuart D. Guest [a], Hossein Izadi [a], Ata Kamyabi Gol [a], Gentry Wood [a]

[a] Canadian Centre for Welding and Joining, University of Alberta, Edmonton, Alberta T6G 2V4, Canada
[b] Apollo Clad
[c] Ulterra Drilling Technologies

ARTICLE INFO

Article history:
Received 3 June 2013
Accepted 7 June 2013
Available online 29 July 2013

Keywords:
Welding
Overlays
Wear protection
Carbides
Cladding
Hardfacing

ABSTRACT

This paper presents a comprehensive survey of welding processes used to deposit wear resistant overlays. It is based on both literature review and research work performed at the Canadian Centre for Welding and Joining. The focus is on the two most popular material systems used for wear resistant overlays: nickel-base with the addition of tungsten carbide particles, and iron-base in which chromium carbides of the form M_7C_3 nucleate during solidification. The processes surveyed in detail are plasma transfer arc welding, submerged arc welding, laser beam welding, gas metal arc welding-related processes using tubular wires, oxy-acetylene flame brazing, and the still-experimental applications of friction stir processing. Cost and market are key factors influencing technical decisions on wear protection overlays, but the information is scarce and often tightly guarded. An informal survey from our industrial partners is included.

1. Introduction

Wear mitigation is at the core of many resource-based industries, which rely heavily on wear resistant materials for extraction and processing, since equipment must endure particularly aggressive conditions which require abrasion, corrosion, and erosion resistance. The estimated cost of wear to Canadian industry is $2.5 billion a year [1]. In the oil sands operations of Northern Alberta, the costs of down time in any of the production lines are estimated to be $3–6 million a day [2]. For a representative oil sands operator, wear replacement parts and labor involve more than $40 million per year. Similar situations can be found in the mining and pulp industries, and the key to maximizing the reliability and up-time is to apply the most wear resistant and thickest coatings available. Using an advanced wear resistant overlay over a conventional steel component or substrate also offers significant savings in terms of material cost and manufacturability.

To reduce wear in applications involving abrasion, materials with high hardness such as carbides are often favored over metals. However, pure carbides perform particularly poorly under impact loading because of their poor fracture properties; also, carbide materials cannot be readily made into complex components or geometries. One of the approaches to combining the superior wear properties of ceramics with the formability of metals is through weld deposited overlays, which combine the resistance to abrasion of carbides with the toughness of a metal matrix, all deposited on top of tough structural steel.

This paper focuses on the welding-based manufacturing processes to create overlays. Spray processes such as high velocity oxygen fuel (HVOF), plasma-spray, or cold-spray are outside the scope of this paper. The following sections present a brief overview of materials systems typically used for wear resistant overlays and a detailed description of the key processes used to deposit these materials systems: plasma transfer arc welding, submerged arc welding, laser beam welding, gas metal arc welding-related processes using tubular wires, brazing, and friction stir processing.

2. Materials systems

This section provides an overview of the materials systems most frequently used in weld-deposited wear resistant overlays. The most common ones are the Ni–WC and CCO systems. Other

Abbreviations: CCO, chromium carbide overlay; CCWJ, Canadian Centre for Welding and Joining; CNC, computer numeric control; CTWD, contact tip to workpiece distance; CV, constant voltage; FCAW, flux core arc welding; FSP, friction stir processing; FSW, friction stir welding; GMAW, gas metal arc welding; GTAW, gas tungsten arc welding; HAZ, heat-affected zone; HI, heat input; LBW, laser beam welding; MCAW, metal core arc welding; PPE, personal protection equipment; PTAW, plasma transferred arc welding; SAW, submerged arc welding; SMAW, shielded metal arc welding.

* Corresponding author at: Patricio Fernando Mendez, Canadian Centre for Welding and Joining, University of Alberta, Edmonton, Alberta, Canada T6G 2V4. Tel.: +1 780 248 1587.
E-mail address: pmendez@ualberta.ca (P.F. Mendez).

1526-6125/$ – see front matter © 2013 The Society of Manufacturing Engineers. Published by Elsevier Ltd. All rights reserved.
http://dx.doi.org/10.1016/j.jmapro.2013.06.011

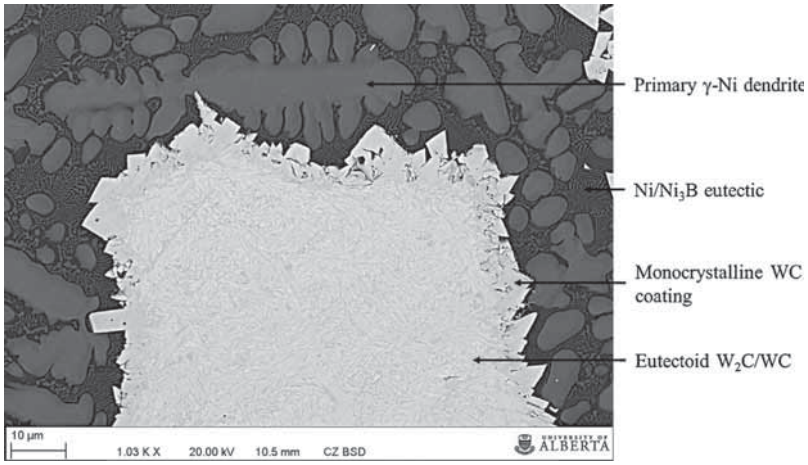

Fig. 1. Backscattered SEM micrograph depicting typical microstructures obtained using GMAW and hot-wire GMAW. Phase compositions identified through EDX.

materials systems available are mentioned toward the end of the section. Ni–WC and CCO represent ends of a spectrum in costs, wear performance, and deposition challenges. Ni–WC is among the most expensive systems, with best wear performance, and is unique in that the carbides must be introduced in the melt, as they do not form during solidification and cooling. In contrast, CCOs are among the less expensive of carbide-based overlays, with lower wear resistance, and with carbides nucleating from the melt.

2.1. Nickel–tungsten carbide (Ni–WC)

Tungsten carbide is typically used as part of a composite overlay with a matrix made of nickel with alloy additions of boron, silicon, and often chromium. The Ni–WC material system differs from other NbC, TiC, B_4C, and CCO hardfacing overlay systems in that the tungsten carbides are not formed in situ during solidification, but rather must survive the welding thermal cycle.

The wear properties of Ni–WC wear resistant overlays lies in the presence of the tungsten carbide. These carbides have high hardness values and uncommonly high toughness compared with other carbides. Dissolution of the tungsten carbide particles into the molten matrix greatly decreases the wear resistant properties of the overlay, requiring the deposition of the metal to be performed with the minimum possible melt temperature.

The Ni–WC material system is typically deposited with PTAW or laser beam welding due to their exceptional HI control. The extreme sensitivity of tungsten carbide to heat eliminates higher productivity processes involving hotter melts and longer cooling times, such as SAW, from being used.

2.1.1. Carbide morphology

The majority of tungsten carbide utilized in conventional hardfacing processes is comprised of "cast and crushed" eutectoid W_2C/WC particles with ~3.7 to 4.1 wt% carbon, which is formed through conventional casting and crushed to size. This process yields angular particles that are comprised of a eutectoid mixture of W_2C and WC phases with hardness ranging between 2200 and 2600 HV [3,4]. Eutectoid carbides are commonly distinguished from other types by the alternating W_2C and WC lamellae in the carbide microstructure.

A variation of the eutectoid carbides, typically called "macrocrystalline" tungsten carbide, is manufactured by carburizing eutectoid W_2C/WC carbides at elevated temperatures to increase the carbon percent to 6.1 wt% (stoichiometric mono-crystalline WC). The carburizing process is preferred over casting at high carbon contents because it avoids carbon segregation and formation of graphite in the carbide microstructure. The mono-crystalline tungsten carbide is more resistant to high temperature dissolution than the eutectoid variants but has a lower overall hardness, typically 1200–2100 HV. Mono-crystalline tungsten carbide particles are not necessarily single crystals.

Both the mono-crystalline WC and eutectoid W_2C/WC carbides are typically angular-shaped and found in size ranges from 40 to 200 μm for arc welding applications; larger variants are also possible.

Recently, a third type of carbide has been developed to specifically address the preferential dissolution of the eutectoid carbides. This carbide is comprised of a eutectoid W_2C/WC core surrounded with a thin layer of mono-crystalline WC obtained through high temperature partial carburization [5]. The mono-crystalline WC outer shell is believed to help decrease detrimental carbide dissolution in PTAW overlays [6–8].

The lower overall HI and rapid cooling rates associated with laser produced overlays allows for the use of spherical fused tungsten carbide particles. The manufacturing of spherical fused tungsten carbide particles is a tightly controlled process in which graded cast and crushed carbides are utilized as the feed stock [9]. Through a series of controlled atmosphere heat treatments, the cast and crushed carbide acquires a spherical shape with a fine "feathery" (possibly metastable) microstructure of overall composition WC_{1-x} [9]. This process results in fully dense spherical carbide particles with increased toughness and a hardness that ranges between 2700 and 3400 HV [10]. The WC_{1-x} microstructure is unstable at high temperatures and requires high cooling rates to prevent phase transformations resulting in excessive carbide dissolution.

2.1.2. Matrix metallurgy

Ni–WC consumables are typically available with a NiCrBSi or NiBSi matrix alloy. The matrix microstructure is typically comprised of soft primary nickel dendrites (~350 HV) while the inter-dendritic regions are comprised of hard borides, carbides, and silicides[11] (~500 to 800 HV) as can be seen in Fig. 1 [7]. The hardness and wear resistance of the matrix is significantly improved by the presence of the inter-dendritic phases [12]. Boron addition decreases the melting temperature of the alloy system and produces a wide solidification temperature range, forming hard Ni_3B phases and decreasing the minimum HI required for fusion of the substrate [13]. The chemistry of the matrix and temperature cycle have a large effect on the level of carbide dissolution [7,14]. Previous studies with PTAW and mono-crystalline tungsten carbide have shown that increasing levels of chromium in the matrix (>8 wt%) leads to excessive carbide dissolution and poor wear

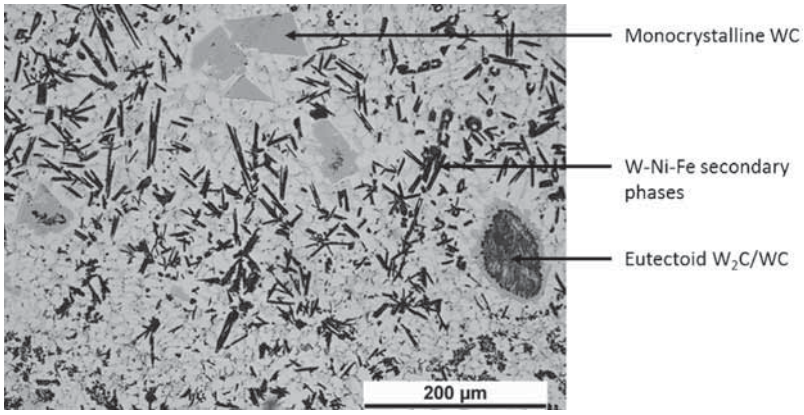

Fig. 2. High HI globular transfer GMAW weld with mixed carbides showing excessive dissolution and re-precipitation of deleterious W–Ni–Fe secondary phases.

performance [7]. The re-precipitated carbides have low toughness, as shown in Fig. 2. After dissolution of the carbides, the tungsten and carbon in solution will re-precipitate as small complex carbides next to the primary carbides as shown in Fig. 3. Re-precipitated carbides increase matrix hardness, but decrease matrix wear resistance, causing chipping and higher wear rates [15].

2.2. Chromium carbide (CCOs)

CCOs consist primarily of iron, chromium and carbon with small amounts of other alloying elements such as manganese, silicon, molybdenum, boron, nickel, and copper. The resulting microstructure consists of M_7C_3 carbides and austenite [16–19]. Silicon is usually kept below 1 wt% to reduce the tendency of pearlite to form. High cooling rates along with the presence of austenite stabilizing elements such as nickel, manganese and copper lead to a high fraction of retained austenite in CCOs. Chromium also plays a role in retaining austenite as it helps slow the rate of austenite decomposition. Even though austenite stabilizers help prevent the formation of brittle phases, the addition of these elements should be kept to a minimum due to their detrimental effect on wear resistance of the CCO [19,20].

CCOs have two common microstructures: hypereutectic and hypoeutectic. Hypoeutectic alloys are more corrosion resistant and contain less carbon (~2 to 3 wt% C) than hypereutectic alloys which usually contain greater than 3 wt% carbon and 11 wt% chromium. Typically, hypereutectic alloys possess greater wear resistance than hypoeutectic alloys due to the higher fraction of carbides in these CCOs and so, are more readily used as wear resistant overlays. It is important to note that hypereutectic alloys may show hypoeutectic microstructure features close to the fusion line because of dilution in this region [15–18,21–28].

Wear resistance of the CCOs depends greatly on the morphology, orientation, volume fraction, size and chemistry of carbides. Carbon plays the most crucial role in the wear resistance and hardness of the overlay [22,24,29–31].

Preliminary experiments using similar compositions with varying HI through LBW, PTAW, MCAW, and SAW have resulted in CCOs with similar microstructures, suggesting that cooling rate might be of secondary relevance [32].

2.2.1. Carbide morphology

CCOs get their main wear resistance from M_7C_3 carbides and unlike tungsten carbides in Ni–WC overlays, the M_7C_3 carbides form during solidification of the overlay weld pool. These overlays are not as wear resistant as the tungsten carbide overlays. CCOs contain large amounts of chromium which can provide them with some corrosion resistance.

The "M" in M_7C_3 indicates that a number of different carbide forming elements (iron and chromium having the highest quantity) can be present in the carbides. By increasing the carbon and chromium content of the CCO (with carbon having a greater effect), the total volume fraction of carbides and wear resistance of the overlay is increased [16–19].

A typical microstructure of a hypereutectic CCO with hexagonal shaped primary M_7C_3 carbides is shown in Fig. 4. Each of the large primary carbides grow as a single crystal in the direction of heat flow while the eutectoid carbides are mainly polycrystaline [18,23].

Recent advances to increase the wear resistance of CCOs involve the use of secondary carbide formers such as niobium, tungsten,

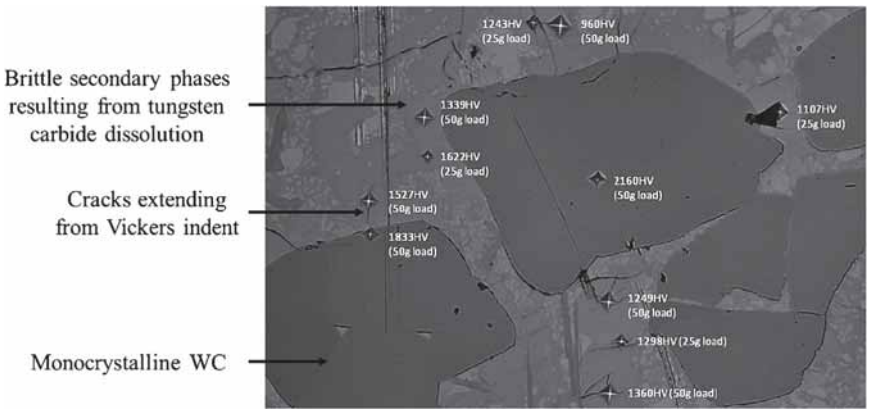

Fig. 3. High chromium matrix alloy resulting in carbide dissolution. Secondary phases are brittle and fracture under Vicker's hardness testing with low force (25–50 g) [7].

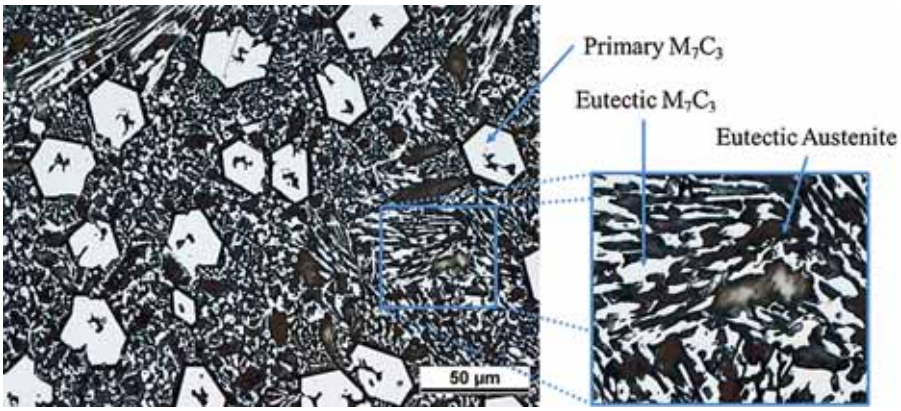

Fig. 4. A typical hypereutectic microstructure of a CCO.

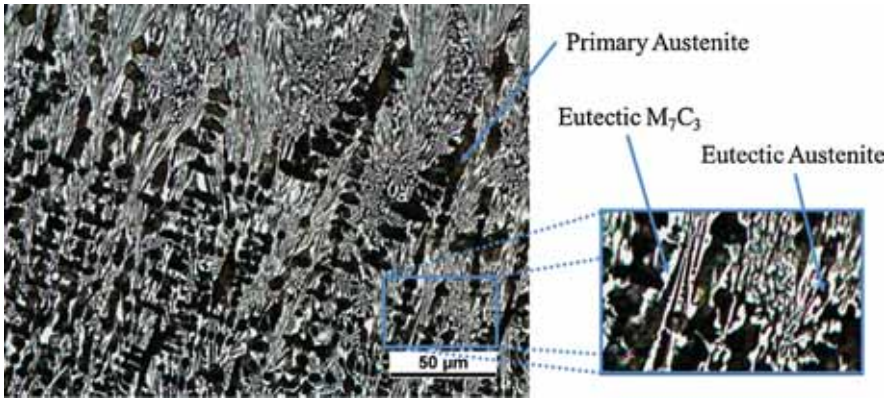

Fig. 5. A typical hypoeutectic microstructure of a CCO overlay.

vanadium, boron, and titanium. Boron is added to the alloy to promote the precipitation of hard phases either by adding boron to M_7C_3 carbides or forming new borides such as $M_{23}B_6$, M_3B, M_2B, and M_3B_2. Boron is believed to refine the size of M_7C_3 carbides by decreasing the solubility of carbon in the austenite matrix. TiB_2 acts as a nucleation site for carbides and therefore, has been added to flux core wires to increase the number of fine TiC–TiB_2 particles in CCOs. In addition to having excellent carbide forming properties, niobium, vanadium and titanium also increase the wear resistance by refining the grain size of the austenite matrix [20,21,33–35]. Table 1 compares some of the major properties of typical reinforcing carbides used in overlays, also including carbides beyond those typically used in CCOs.

2.2.2. Matrix metallurgy

The solidification path of any hypereutectic alloy starts with the formation of primary M_7C_3 carbides followed by the eutectic transformation of liquid to austenite and M_7C_3. A thin layer of austenite surrounding the primary carbides can be seen in Fig. 4. It is believed that this thin layer is directly related to the depletion of chromium in the liquid surrounding the primary carbides [16]. The eutectic surrounding the primary carbides is often referred to as the matrix.

Hypoeutectic alloys first solidify as primary austenite and then as a eutectic of austenite and M_7C_3 carbides between the large primary austenite dendrites. The typical microstructure of a hypoeutectic alloy is shown in Fig. 5.

Table 1
Properties of reinforcement carbides [2].

Carbide	Hardness (HV)	Density (kg/m^3)	Melting point (°C)
B_4C	3670	2500	2450
TiC	3000	4900	3100
W_2C	3100	17,200	2785
VC	2900	5700	2700
NbC	2000	7800	3600
WC	2200	15,700	2870
Cr_7C_3	1630	6900	1755
Cr_3C_2	1400	6700	1800
Fe_3C	1020	7500	1252

2.2.3. Process considerations

CCO is a very versatile wear protection overlay that can be deposited with a wide range of processes. Taking into account that SAW is the most common method to deposit CCOs, this section revolves around considerations and references to less typical processes used for CCOs not described in later sections.

LBW or PTAW of chromium carbides is possible but the large cost of equipment does not make it conducive to being used for CCOs when high quality overlays can be made using less expensive processes. More research, however, may be needed to look into the possibility of LBW for specialty applications because of its ability to produce relatively smooth surface finishes and extremely low dilution amounts. It is possible to get deposition rates of 20 lb/h with laser welding CCOs.

CCOs can be deposited using a wide variety of available SMAW consumables. Advantages of SMAW for CCOs include portability of the machine and ease of use for repairs. Drawbacks include low productivity compared to other processes. SMAW of CCOs can reach deposition rates of up to 30 lb/h [16,27,36–38]. Typical range of operating parameters for SMAW deposition of CCOs are around 160–130 A, 20–27 V, 180–200 mm/min travel speeds, and 3.2–4.8 mm diameter electrodes [16,36].

CCOs can be deposited in GTAW experimental setups by weaving a GTAW torch over a pile of alloying powders. This is because GTAW allows for easy manipulation of composition and other welding parameters [25,39,40]. Typical operating ranges for CCOs deposited by GTAW fall in between 14 and 15 V, 100 and 1220 A, and 30 and 1100 mm/min travel speeds [25,39,40].

2.3. Market considerations

Market numbers are very important to make commercial decisions and are often tightly guarded. This subsection summarizes an informal survey performed with suppliers of Ni–WC overlay consumables. For confidentiality reasons, the original sources often cannot be named.

Worldwide, it is estimated that Ni–WC powders only account for approximately 5% of the overall wear protection overlay market, with the balance being comprised of single component hardfacing material systems such as CCOs and Stellite. Conversely, the cost of a Ni–WC overlay can be as much as 10–15 times the cost of a CCO of similar geometry. Ni–WC alloys can be very expensive. Powders by themselves cost approximately $150/kg, and this accounts to only 30% of the total cost [2], with the other 70% related to the cost of application.

The bulk of the demand for single component hardfacing overlays can be traced to high volume, narrow focus operations, such as hardfacing of engine valves and valve bodies for chemical and subsea systems, which requires approximately 500 tons/year worldwide. Excluding the volume share attributed to engine valves, Carbide based overlays account for approximately 25–30% of industrial usage.

Some powder producers estimate that for both PTAW and laser processes, Ni–WC hardfacing powders (both angular and spherical tungsten carbide) have a volume potential of 30 tons/year in North America. This amount of tungsten carbide comprises about 60% angular and 40% spherical carbides; there are indications that the ratio might reverse by 2016. Other powder suppliers present a somewhat different estimation, with approximately 85% of the carbide manufactured to be used in PTAW operations, and the remaining 15% attributed to laser overlays, with approximately 66% of the spherical carbide produced, utilized in laser cladding operations.

CCOs are typically inexpensive compared to tungsten carbide overlays, leading them to being used in larger applications such as truck bed liners and pipeline slurry transport [17]. At peak production, the market for chromium carbide pipe overlays in the oil sands in Canada are roughly 70–80 million dollars a year. The ratio of CCO piping compared to plates is estimated to be between 3:1 and 4:1.

3. Plasma transferred arc welding

3.1. Description of process

PTAW is a specialty welding process used for the deposition of wear resistant protective coatings on to the surface of metals. The PTAW process is similar to the GTAW process in that an arc is formed between a tungsten electrode and base metal with a shielding gas being flooded around the weld pool to protect the weld pool from outside contaminants. The PTAW torch is quite bulky compared to GTAW as it uses a water-cooled arc constrictor that increases the energy density of the arc. Tungsten electrode setback, orifice diameter and plasma gas flow rate are some of the other factors that help increase the energy density of the arc. Instead of utilizing wire-based consumables like GMAW and SAW, PTAW typically uses powder consumables blown into the arc periphery using a mechanical and powder carrier gas feeding system. A schematic of the process as it is used for overlays is shown in Fig. 6.

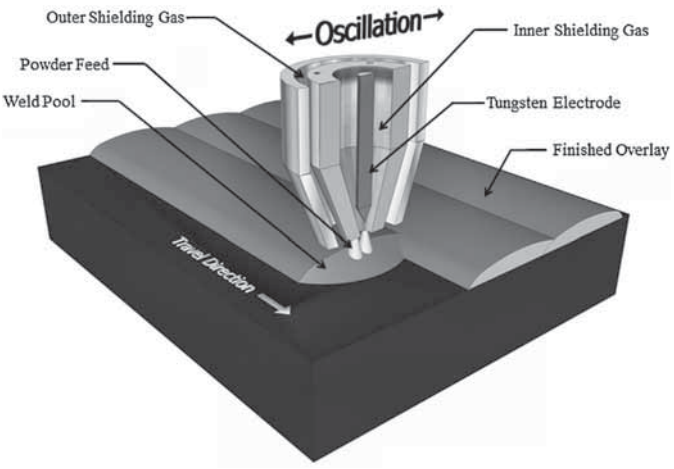

Fig. 6. Schematic of the PTAW process used for depositing wear resistant overlays.

Since the deposit material is in powder form, the PTAW process does not require as high HI as other arc based overlay processes for equivalent amounts of deposition. As such, the PTAW process has far less dilution into the substrate (<10%) than other arc based processes and produces overlays with extremely strong metallurgical bonds to the substrate. The overlays produced are also relatively free of defects.

The PTAW process has far more flexibility than other arc based overlay processes in terms of ability to produce overlays with any desired composition. This is due to the use of powders as the deposit material, which allows for free mixing of any powder types so long as there is consistency in the powder sizes used. Wire-based processes are limited to the specific elemental composition produced by the manufacturer, virtually eliminating the ability to create a "custom" overlay optimized for specific in-service conditions.

Typical deposition rates in industrial uses range from approximately 2–30 lb/h, although some specialty torches can reach up to 50 lb/h. The PTAW process is an automated process that is not done manually. Typical heat intensity for the PTAW process can range up to 15 kW [3].

Safety considerations for PTAW are very similar to other arc welding processes including full length pants, closed toed shoes, safety glasses, welding jacket, and a welding helmet. The highly constricted arc of PTAW also requires proper workstation shielding to protect other welders from its intense light. Fig. 7 shows a PTAW machine used for research purposes.

3.2. Typical materials systems

There are several different material systems that are common to PTAW. The most common type of wear resistant overlay used is Ni–WC.

Another possible material system for PTAW is CCOs. These overlays are commonly used as wear and corrosion protection of equipment used in the oil sands and have a much lower cost than Ni–WC. Minimal work has been done looking into PTAW deposition of CCOs [24]. The relatively high price of PTAW equipment compared to that of SAW, FCAW, or SMAW often makes economically impractical to deposit relatively low value added overlays such as CCOs. PTAW, however, may be advantageous in overlay research because of its flexibility in adjusting the feed powder composition. It is also capable of producing overlays with extremely low dilution.

Other materials systems used in PTAW include Inconel alloys, Colmonoy alloys, Stellites, and NiCrBSi alloys. The metallic NiCrBSi

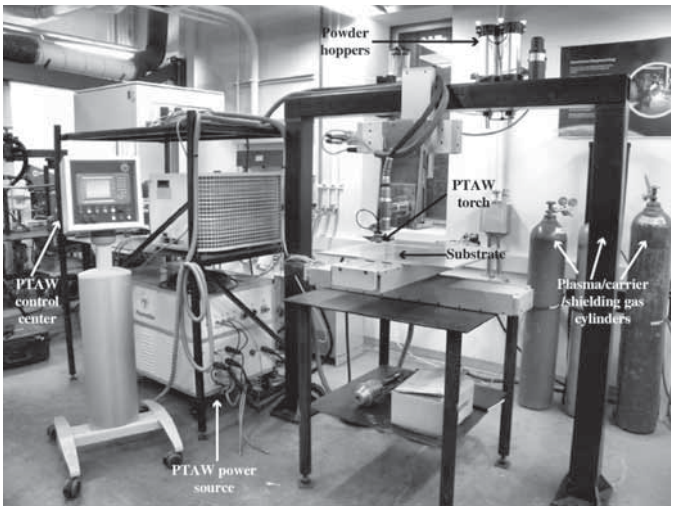

Fig. 7. PlasmaStar PTAW machine at the CCWJ. This custom machine is capable of higher currents than most industrial equipment (up to 500 A and 50 lb/h deposition rate).

coatings are widely used and provide a large variability of properties depending on several factors, including but not limited to composition and welding parameters. Matrix alloys of cobalt and carbide systems outside tungsten or chromium, for example boron carbides, have also been tested but are used in much smaller amounts.

3.3. Typical applications

PTAW is a specialized process, very popular for depositing tungsten carbide reinforced alloys for mining applications such as oil sands of Canada or coal mining worldwide. The applications are typically related to ground engagement requiring the maximum possible wear resistance, justifying the high cost. Teeth and lips of "buckets" (the large shovel used in excavation of oil sands), as well as the contact part of drilling equipment are amongst the applications.

Due to the automated nature of the process, it is not possible to perform PTAW welds outside a dedicated shop, and as such it cannot be used for small overlay repair work. There is also some PTAW work done relating to the oil sands involving CCOs, but they are more commonly welded using the SAW process.

On a larger scale, PTAW is used for Inconel weld overlays all around the world. These overlays are nickel based and have a large variability in composition and uses.

3.4. Typical challenges

There are several key challenges that are faced when depositing hardfacing overlays with the PTAW process. The two main challenges are the control of the dilution/dissolution and settling of carbides to the bottom of the weld with the Ni–WC family of overlays.

The importance of dilution is paramount, as it can significantly alter the substrate properties and remove much of the wear resistance of the overlay. The amount of dilution present in welds is directly related to the HI used during the welding process. The HI itself is a function of the arc current and travel speed in PTAW.

When depositing Ni–WC overlays, the settling of carbides produces a "denuded" zone of low wear resistance at the top of the deposited layer [2]. The settling of tungsten carbide is attributed to two main factors: density and solidification time. Tungsten carbide is approximately twice as dense as the surrounding Ni-based

Fig. 8. Typical cross section of Ni–WC overlay deposited with PTAW.

matrix, leading to settling at the bottom of the overlay. With long solidification times resulting from high HI, the weld pool remains liquid for longer periods of time. This will allow the dense tungsten carbides sufficient time to settle at the bottom, producing a denuded region at the overlay surface devoid of carbide.

3.5. Typical process parameters

Shown below in Table 2, are three different sets of PTAW parameters for Ni–WC overlays.

3.6. Typical microstructures

Fig. 8 shows the cross section of a single bead of Ni–WC overlay deposited by PTAW with typical parameters. A carbide-free layer can be observed at the top; this denuded layer is a consequence of carbide settling and has very low wear resistance. The rest of the overlay is relatively homogeneous and densely packed with carbides. A common target in practice is to achieve a volumetric fraction of carbides of 50%. Fig. 9 illustrates the typical microstructure of a CCO deposited with PTAW. Although not visible with the magnification chosen for this figure, there is no settling of carbides in PTAW deposited CCOs due to the nature of their nucleation and growth during solidification.

4. Submerged arc welding

4.1. Description of process

SAW is an attractive process for the manufacturing of overlays because of its productivity and high deposition rate. Typically, when using SAW for CCOs, a powder that is high in alloying elements such as chromium, carbon, manganese, and molybdenum is placed down in front of the welding head. The welding torch and flux head then moves forward over the powder with a low alloy steel wire while performing a weave function in order to increase the width of the weld bead. Conventional SAW flux is used to help protect the weld pool from the atmosphere. The ability to easily adjust the final composition by altering the composition of the

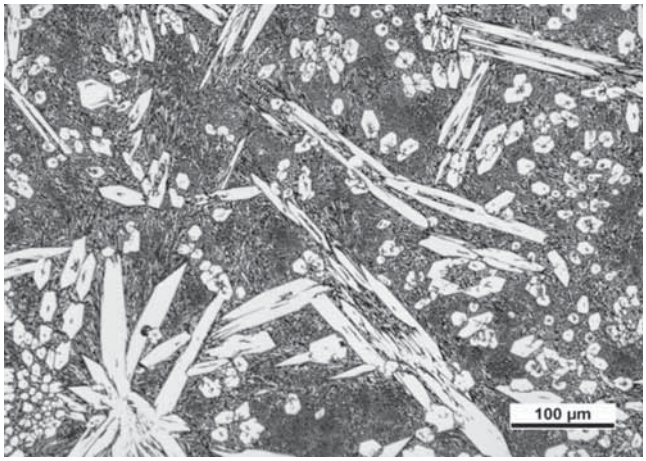

Fig. 9. Typical microstructure of CCO deposited with PTAW.

Table 2
Typical parameters used in PTAW process of Ni–WC overlays.

Parameter	Set #1	Set #2	Set #3
Current (A)	130	150–160	150–200
Voltage (V)	23.5	25	25
Plasma gas flow (lpm[a])	2	N/A	2
Powder gas flow (lpm[a])	N/A	N/A	3
Shielding gas flow (lpm[a])	9	12	10
Carrier gas flow (lpm[a])	1.4	N/A	N/A
Powder feed rate (g/min)	N/A	25	91
Travel speed (mm/s)	3.81	0.3–0.5	4.2
Stand-off (mm)	N/A	N/A	8
Reference	[2]	[41]	Typical at CCWJ

[a] lpm: liters per minute.

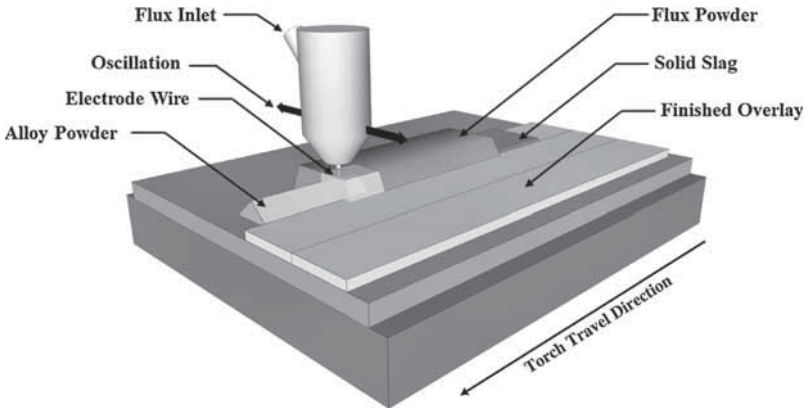

Fig. 10. Schematic of the SAW process used for depositing wear resistant overlays.

powders is an advantage of using this process. The deposition rate of SAW can be upwards of 50 lb/h (23 kg/h). A schematic of the process as it is used for overlays is shown below in Fig. 10.

CCOs are often produced using SAW on large plates that are then worked, plasma cut, and welded into desired shapes. Another common use is cladding of pipes. For large diameters this can be done using SAW but for smaller internal diameters MCAW/FCAW is commonly used. Another advantage of the SAW process is that after the initial setup, the required operator skill is much lower than for manual processes; The process is also highly automated which helps to increase the productivity of the process, these are very important advantages in manufacturing situations facing skilled labour shortages [27]. Fig. 11 illustrates an industrial setup of the SAW process for applying overlays on plates.

Recent innovations in SAW cladding include the Lincoln Cladiator which uses one power supply and multiple GMAW wires simultaneously to increase the deposition rate and cross-sectional homogeneity of SAW deposited overlays. The Lincoln Cladiator is shown in Fig. 12.

Safety considerations in the SAW deposition of wear resistant overlays include the use of particulate masks while handling the powders and welding in addition to the usual welding PPE. Proper local ventilation is also important. Because of the protective slag, concerns about hexavalent chromium are much smaller than in open arc processes.

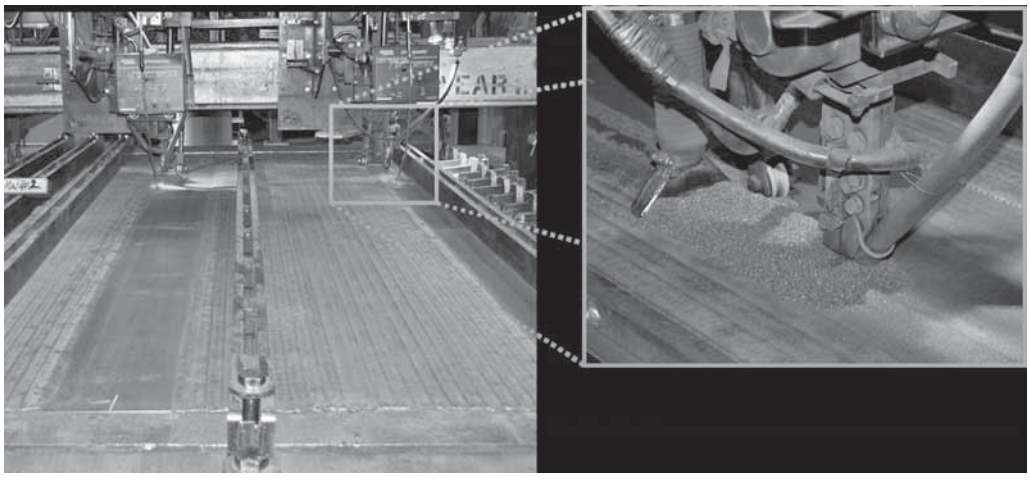

Fig. 11. Industrial CCO production with two SAW welding heads on a single plate.
Source: Courtesy of Wilkinson Steel and Metals.

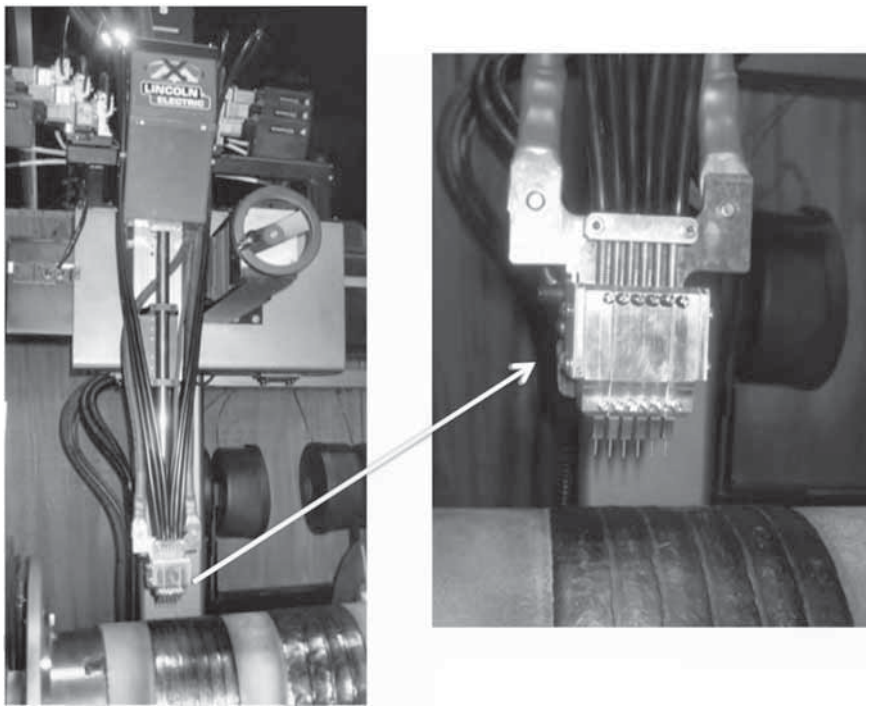

Fig. 12. Lincoln Cladiator, which uses a SAW power supply with multiple GMAW wires to deposit overlays.

4.2. Typical materials systems

The most commonly produced product using SAW is CCOs. Tungsten carbide overlays are not produced using SAW because of the high weld pool temperatures associated with SAW which would lead to the dissolution of the tungsten carbides.

4.3. Typical applications

Typically SAW deposited CCOs are used in circumstances where they will be undergoing abrasion, impact, erosion, and corrosion [22,31,36,42]. They are used in a large number of industries including mining and mineral processing, cement production and pulp and paper manufacturing [18,23,31]. Some specific examples of their uses in the oil sands include crusher teeth, hydro transport screens, and centrifugal pumps [42,43]. The vast majority of CCO plate is produced using SAW.

4.4. Typical challenges

CCOs commonly have transverse cracking that results from contraction of the weld bead during cooling [17]. This is commonly referred to as relief cracking and is acceptable as long as the crack width stays below designated sizes and does not continue into the base plate. Small amount of relief cracking is often interpreted in practice as an insufficient amount of carbides in the bead. Fig. 13 shows a typical SAW CCO overlay with multiple relief cracks in the surface.

A challenge of SAW deposition of overlays is the large amount of dilution associated with its relatively high HI. Dilution causes the composition of the overlay to become leaner (making a hypereutectic alloy behave like a hypoeutectic), and for CCOs, results in fewer carbides, and ultimately decrease the overlay wear resistance. Another problem that can arise with the SAW process is the large amount of distortion in the plates during welding. To overcome this problem, heavy duty clamping must be employed along with careful observation from an operator to ensure correct welding head to plate distances (correctly named CTWD) are maintained.

A downside to SAW is that it can only be performed in the flat position. The large equipment involved in SAW overlays cannot be used manually and field repairs of worn components are not possible. Repairs during the manufacturing of SAW CCO plates are typically done using MCAW/FCAW wires with similar compositions as the base CCO material. Some FCAW wires are 'all position' capable. This process still suffers from the problem of dilution that SAW encounters but in most cases the welding procedures of the overlay accounts for this problem by calling for minimum of 2–3 layers of the overlay. One drawback to the MCAW/FCAW wires is that they tend to experience problems with spalling of thicker sections made with multiple passes.

4.5. Typical process parameters

Typical operating ranges used during the SAW deposition of CCOs are in the range of 30–40 V and 500–700 A. Welding of CCOs is commonly performed in CV welding mode. The wire feed speed

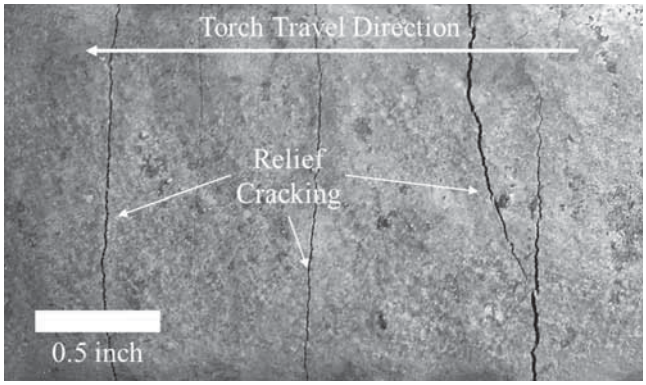

Fig. 13. Relief cracking in SAW deposited CCOs.

Table 3
Comparison of working parameters between SAW and other welding processes.

Process	Voltage (V)	Current (A)	Speed (mm/min)	HI (kJ/mm)	Reference
LBW	3000–6000[a]		240–420	0.5–0.9	CCWJ lab
PTAW	25	200	225	0.8	CCWJ lab
SAW	30–40	500–700	200–300	3–8	CCWJ lab
SMAW	22–23	130–160	195–240	0.88–0.92	[16], CCWJ lab
FCAW and GMAW	24–36	200–500	200–825	0.68–2.95	[29,31,35,44], CCWJ lab
GTAW	14–15	100–220	30–100	0.84–6.6	[25,39,40]

[a] Measured in units of watts.

and alloy powder amount are varied to control the resulting final composition. Operating parameters should also be chosen to ensure proper melting of all the powder, a good surface finish and easy slag detachability. The weld beads can be two inches in width and vary in height of 3/16″ to 3/8″ thick. To achieve thicker sections multiple passes can be performed. These weld beads are placed next to each other with a small overlap and are continually laid down until the desired width of plate is covered. Plate sizes can vary depending on component size but in some cases can be up to 8 ft by 20 ft (2.4 m × 6 m). A comparison between typical process parameters in SAW and other welding processes used for overlay deposition are presented in Table 3.

4.6. Typical microstructures

The microstructure of CCOs is not homogeneous, with larger variances than in white cast irons of comparable composition. It is believed in industry that wear performance varies markedly between layers, and specifications are made to account for this; for example, by measuring wear performance at 75% of overlay depth. Measurement of the wear performance at 75% depth will determine the amount of microstructure inhomogeneity caused by excessive dilution. The causes and consequences of layering in CCOs have not been investigated systematically yet, and it is likely that all CCOs produced are suboptimal, as this layering is not a controlled variable in quality assurance procedures.

Fig. 14 shows how dilution and segregation can dramatically change the microstructure from the top to bottom of overlays deposited through SAW. As mentioned before, HI (which controls cooling rate) seems to play a secondary role in microstructural development of CCOs within reasonable range of parameters [32].

5. Laser beam welding

5.1. Description of process

In laser cladding, a laser heat source is utilized to deposit material onto a given substrate that is manipulated relative to the laser

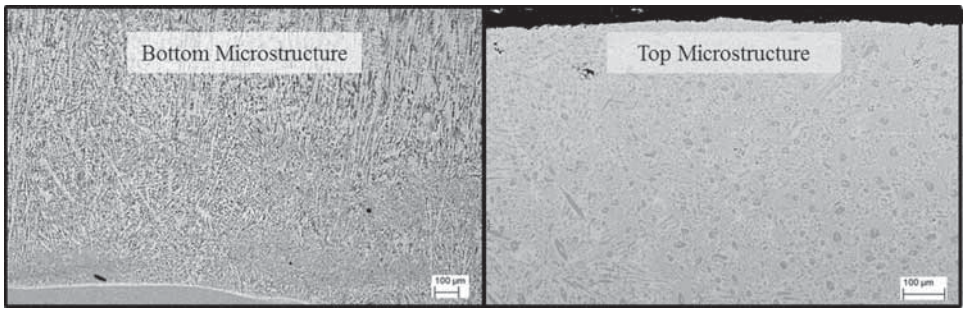

Fig. 14. Typical microstructural inhomogeneity of SAW deposited CCOs. The bottom microstructures are typically hypoeutectic (from dilution) while the top microstructures are hypereutectic, evident by the large fraction of primary M_7C_3 carbides.

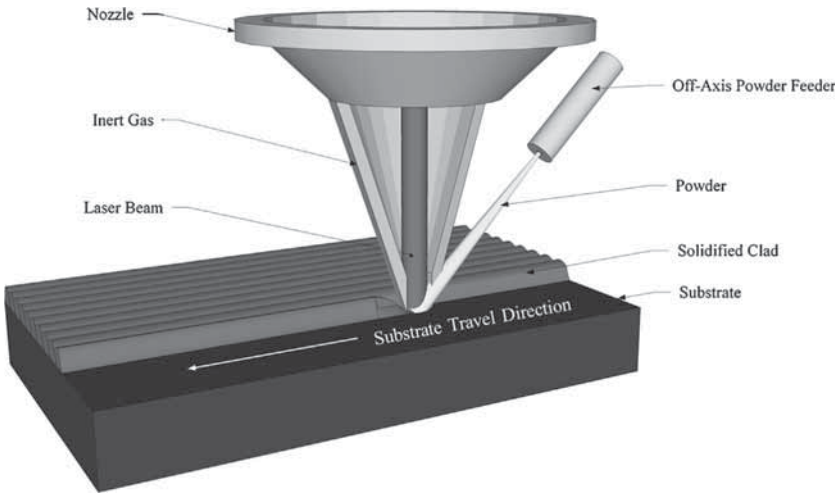

Fig. 15. Schematic of the LBW process used for depositing wear resistant overlays with off-axis feed.

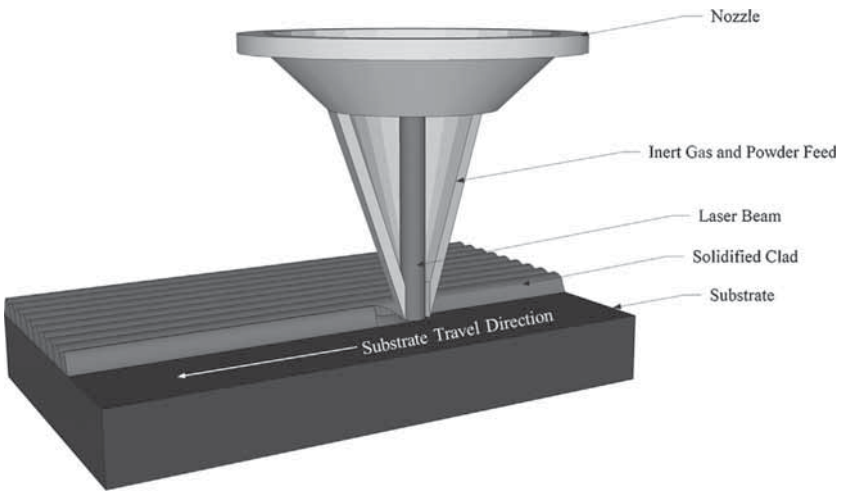

Fig. 16. Schematic of the LBW process used for depositing wear resistant overlays with co-axial feed.

via CNC or robotic assemblies. Industrial hardfacing applications are dominated by powder injection methodologies [4,45–48]; however, significant research has been conducted into a broad diversity of methods of transferring the deposited material to the substrate, such as preplaced powder [49,50] and wire feeding processes [51].

In the powder injection method of delivery, the hardfacing material is delivered to the molten pool by an inert carrier gas through a nozzle assembly that is either 'off-axis' from the laser beam, or co-axial with the incident laser beam. The two types of nozzles are shown schematically in Figs. 15 and 16.

In the case of both the co-axial and off-axis nozzles, the powder is injected into a molten pool created by interactions between the laser, substrate, and inflight powder. Maximum achievable deposition rates for laser cladding processes are determined primarily by the maximum power output of the laser source. Lower power lasers typically utilized in research (500 W–3 kW) can generally support nominal deposition rates that range from tens of milligrams per minute to 30–40 g/min (1.8–2.4 kg/h) depending on the material system being utilized [4,10,45–48]. Higher power lasers generally employed in production (3–10 kW) are capable of depositing up to 9 kg/h without the use of secondary equipment [52]. Fig. 17 shows an industrial setup of a laser cladding system.

Lasers used for welding overlays can create high energy densities resulting in very high thermal gradients within the weld zone. These high gradients result in negligible dilution, low overall HI, minimum part distortion, small heat affected zone, and very fine solidified microstructure. The resulting laser overlay microstructure (both with external carbides or nucleated carbides) is typically very homogeneous compared to other processes.

The advantages of laser processing are the minimal HI, which limits dissolution of the base material and hard-phase particles [14], and also allows for rapid cooling, which promotes fine dispersion and uniform distribution of the hard phases throughout the matrix.

Laser overlay deposition safety considerations are similar to those of mainstream welding operations, with the addition of special eye protection appropriate for the wavelength of laser that is being employed. The longer wavelength radiation associated

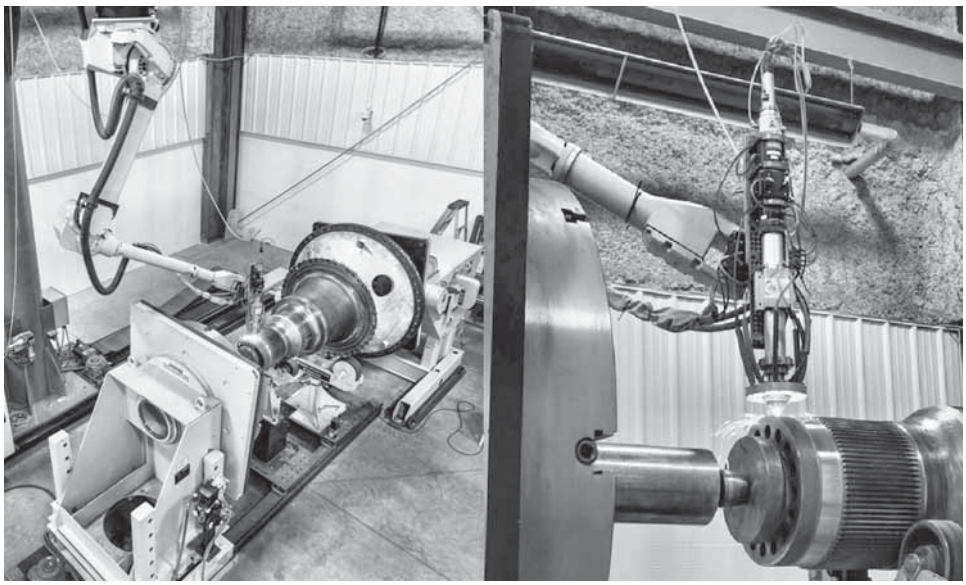

Fig. 17. Photos showing a typical laser cladding set-up. *Left*: Overview showing a large mining component being manipulated with CNC relative to a robotic laser assembly. *Right*: Close-up of cladding head with co-axial powder delivery.
Source: Courtesy of Apollo Machine and Welding Ltd.

Table 4
Typical laser operating parameters.

Laser type/power	Wavelength	Material system	Deposition rate	Operating power	Cladding Speed	Nominal HI
CO_2/6 kW	10.6 μm	NiCrB—WC[a]	1.5–3 kg/h	3.0–5.5 kW	75–200 cm/min(30–80 in/min)	0.10–0.44 kJ/mm
Diode/4–6 kW	1.06 μm	NiCrB—WC[a]	1.5–4 kg/h	1.5–4.5 kW	75–200 cm/min(30–80 in/min)	0.05–0.36 kJ/mm

[a] Spherical tungsten carbide reinforcement.

with CO_2 laser systems (10.6 μm) is absorbed by standard polycarbonate lenses; however, shorter wavelength laser radiation (≈1 μm), such as that associated with diode or Nd:YAG laser systems, can pass through polycarbonate with little or no attenuation. For this reason, shorter wavelength laser systems require special enclosures equipped with window or viewports that possess the appropriate optical density. The Canadian Standards Association (CSA) has set out guidelines for both general laser safety [53], and also for appropriate optical density and tint required for adequate eye protection [54].

Other safety considerations include stray reflections and flying sparks. It is possible for the laser to be reflected off beveled features or sharp corners. These reflections are the result of scattered radiation due to the incomplete absorbance of laser energy by most metals, and are strongly dependent on laser wavelength [55]. This can cause serious and instantaneous burns to individuals who are in the path of the stray radiation. To combat this problem, personnel in close proximity to the laser during cladding should be limited, and all operators should wear appropriate attire (i.e. natural fibers, flame retardant coveralls, etc.) that covers exposed skin. The majority of reflections can be controlled by physically offsetting the laser relative to the surface to bias the reflections in a harmless direction. For example, cylindrical components can be clad slightly off-centre to direct reflections away from the operator.

Additionally, in the province of Alberta, it is required that all lasers that meet Class III or IV laser system criteria must be registered. The classification system is tied to power output, wavelength, etc., and may require the company or organization operating the laser system to provide specialized training and documentation.

5.2. Typical materials systems

Because of the very controlled molten zone, laser overlays have much flexibility in the choice of material system as long as it is chemically and/or metallurgically compatible with the substrate. Substantial research has been dedicated to the investigation of more traditional hardfacing overlays such as composites of tungsten carbide in nickel alloy matrices [4,46,48,56–58] and cobalt based overlays such as Stellite and Tribaloy [47,50,57–59], as well as the development of new materials systems. The more promising areas of research are the use of laser processing to produce exceptionally fine hard phases or functionally graded microstructures via in situ alloying and synthesis [60–63].

However, industrial laser hardfacing overlays for the purposes of wear and abrasion resistance are dominated by the use of tungsten carbide in a NiCrBSi matrix. This material system currently dominates in industry as overlays of this type offer exceptionally good wear properties in combination with good corrosion resistance and low magnetic permeability. Additionally, many variations of this type of material system are commercially available, and it is possible to select products to meet specific industry needs.

5.3. Typical applications

A large fraction of wear resistant laser overlays is for the oil and gas industry, with Ni–WC being dominant. Occasionally, cobalt matrices are used. Special challenges to wear protection overlays are presented in heavy oil extraction, such as in the oil sands of Alberta, which require a new class of wear materials and application processes for the specialized equipment and processes used (such as furnace tubes and elbows for upgrading and separation equipment, Steam Assisted Gravity Drainage (SAG-D), and drilling tools).

The low overall HI of the laser cladding process, coupled with rapid solidification rates serve to limit the dilution of the base material and prevent degradation of the wear and corrosion performance of the overlay. Additionally, the small HAZ associated with the overlay means that the substrate properties are relatively unaffected with negligible part distortion. This has particular importance for tools involving geophysics instrumentation such as mapping while drilling (MWD) and logging while drilling (LWD) tools. These tools utilize highly sensitive magnetic sensors to determine tool location and drilling speed and need to be housed in specialty materials with low magnetic permeability such as high manganese austenitic stainless steels. Any overlays applied to these types of materials must maintain a relative magnetic permeability <1.01 $\mu H\,m^{-1}$. The low HI and low dissolution of composite hard phases such as tungsten carbide, enable laser cladding overlays to be one of the few processes capable of meeting stringent magnetic requirements while providing adequate wear performance.

The same benefits that allow for hardfacing of highly sensitive magnetic parts also apply to laser cladding of high value and critical components in need of refurbishment. Dimensional repair and hardfacing restoration of superalloys such as Inconel 718 and high value alloy castings and forgings (e.g. drilling stabilizers) can also be repaired using this process.

5.4. Typical challenges

Powder utilization ("catchment") efficiency is a major issue related to continuous powder feed systems for laser cladding. Nozzle geometry, clad pool geometry, travel speed, and powder feed rate all influence the fraction of powder that contributes to the overall clad build up. The nozzle geometry, whether co-axial or off-axis, focuses a powder jet on the molten region of the pool. The geometry of the pool is controlled primarily by beam power and travel speed [64]; furthermore, it is required that the size of the molten pool must be sufficiently large [64] to encompass the focal diameter of the powder stream.

Interactions between particles, the beam, inert gas, and molten pool dramatically influence overall clad quality and catchment efficiency [55]. Powder impingement behavior can be classified in three groups: solid particles ricocheting off a solid surface, solid or liquid particles adhering to the liquid surface of the pool, or liquid particles attaching to solid surfaces [65]. The powder impingement behavior is dependent on particle density, distribution, velocity, and the size of the powder stream focal point relative to the molten pool [66].

Another potential challenge with laser cladding is that the process is much more sensitive to part cleanliness than most conventional weld overlay processes. Typically, this involves mechanical cleaning with a pneumatic or electric wire brush followed by an acetone rinse to remove oil residue. Remaining debris will often result in fusion line defects in the form of entrapped oxides. These defects are potential stress concentrations and can

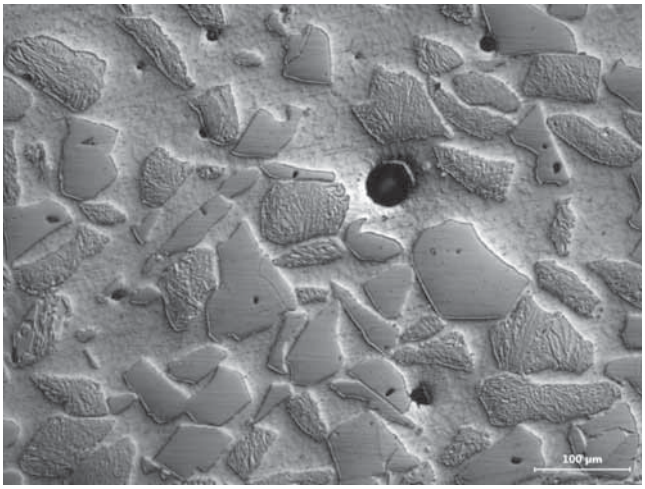

Fig. 18. Microstructure showing the as clad morphology of eutectoid W_2C/WC and mono-crystalline WC angular cast and crushed particles.
Source: Courtesy of Apollo Machine and Welding Ltd.

be the source of non-radial cracking, which may lead to spalling in service.

5.5. Typical process parameters

Typically, operating parameters, such as laser power, powder flow rate, and laser scan rate (cladding speed) are fully automated through the CNC programming; however, operator monitoring and input is still required to ensure part alignment and process quality.

A range of typical laser process parameters are presented below in Table 4. In this table, the nominal HI does not account for line losses in the laser optics, thermal efficiency and catchment efficiency. The range of typical HI for the diode laser process is significantly less than for the CO_2 laser process. This discrepancy is a result of the differences in laser absorptivity for a given substrate for different wavelengths. For example, for low to medium alloy steel, the absorptivity at the CO_2 wavelength lies between 7% and 15%, while for the same material, the diode wavelength will have absorptivity between 50% and 70% of the incident energy [10].

5.6. Typical microstructures

Microstructural images of as-clad angular and spherical tungsten carbide particles are shown in Figs. 18 and 19, respectively.

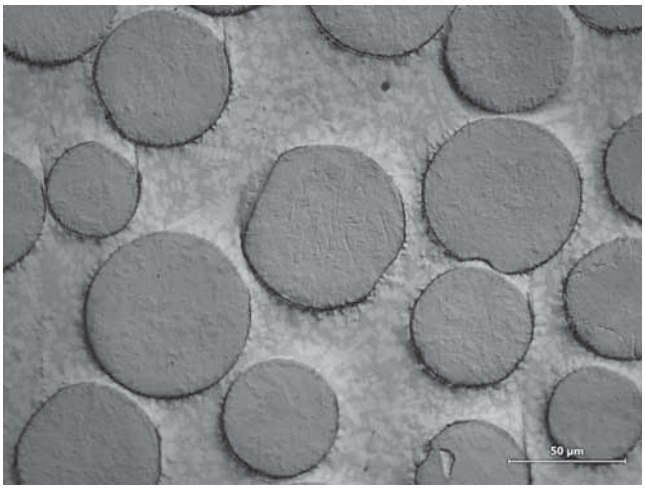

Fig. 19. Microstructure showing spherical WC_{1-x} particles in a Ni–Cr–B matrix.
Source: Courtesy of Apollo Machine and Welding Ltd.

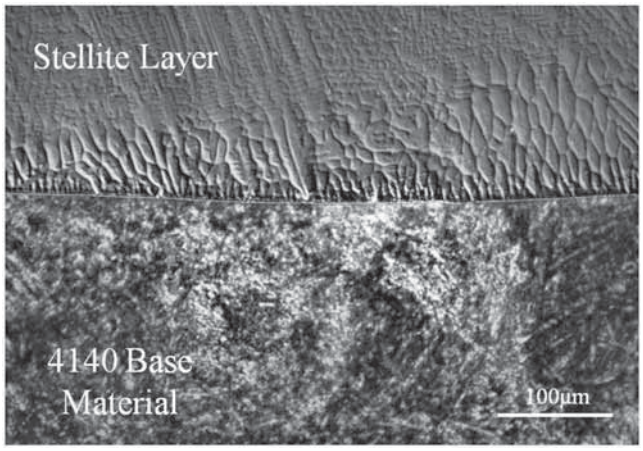

Fig. 20. Microstructure showing the fusion line region of a Stellite overlay applied to 4140 ally steel.
Source: Courtesy of Apollo Machine and Welding Ltd.

Single component clads including superalloys, stainless steels, and cobalt alloys exhibit a typical solidification microstructure of primary dendrites extending perpendicular to the fusion line towards the surface of the overlay. Owing to the rapid thermal cycles of the laser process, the microstructures of the overlays are generally fine-grained and homogenous. Microstructural images showing the fusion line regions of a Stellite overlay on a 4140 alloy steel substrate, and an Alloy 625 corrosion resistant overlay on Inconel 718 are respectively shown in Figs. 20 and 21.

6. Gas metal arc welding family and hot-wire additions

6.1. Description of process

GMAW is a very versatile and widely used welding process. The ease of use, all-position capabilities, compact size, and relatively inexpensive power supplies have made GMAW an attractive deposition method for many wear resistant coatings. A schematic of the process as it is used for overlays and an experimental setup used in the CCWJ lab are shown below in Figs. 22 and 23, respectively.

In this section the focus will be on CCO and nickel matrix, tungsten carbide reinforced (Ni–WC) wear resistant overlays. While CCO consumables have been well documented since their inception, the recent development of tubular nickel-sheathed, tungsten carbide and alloying powder core wires has provided an

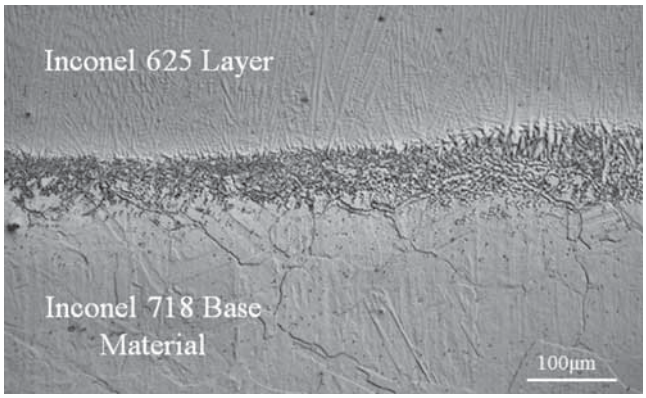

Fig. 21. Microstructure showing the fusion line region of an alloy 625 corrosion resistant overlay applied to an Inconel 718 substrate. Etched with Bell-Jacobs' Reagent (25 mL HCl, 25 mL H_2O, 2.5 mL 30% H_2O_2).
Source: Courtesy of Apollo Machine and Welding Ltd.

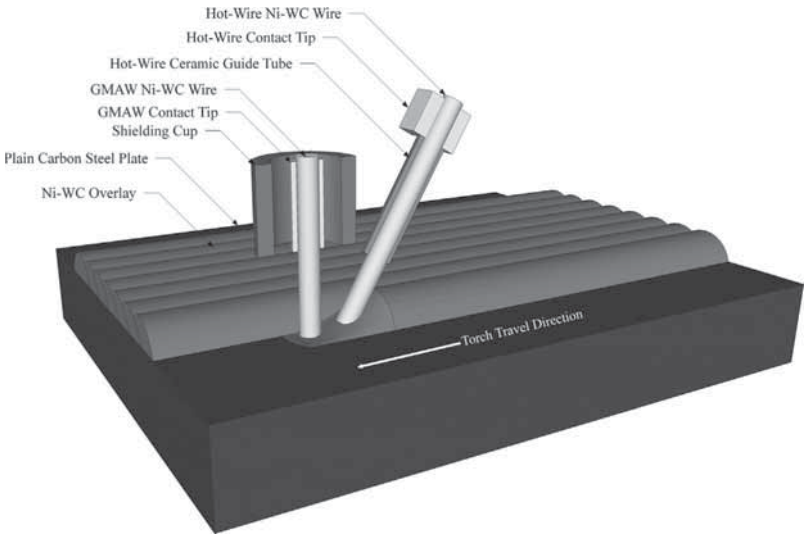

Fig. 22. GMAW and hot-wire torch arrangement for Ni–WC overlay production on a plate surface.

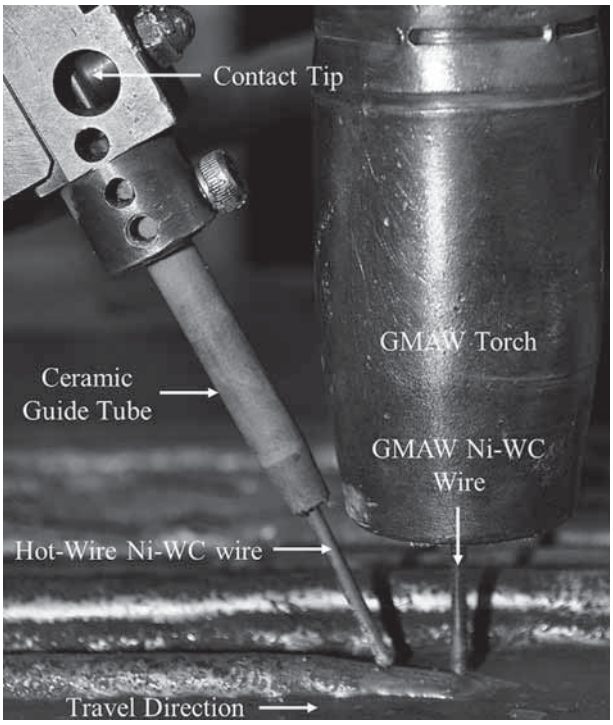

Fig. 23. Hot-wire GMAW torch setup with Ni–WC consumables for both the GMAW and hot wire.

alternative to the standard PTAW and laser cladding processes. Wires are currently manufactured in diameters from 1/16″ (1.6 mm) to 7/64″ (2.8 mm), with the smaller diameters being more commonly used. Currently, there are several manufacturers of Ni–WC wires worldwide, each with large differences in the sheath thickness and internal volume, shown in Fig. 24. The consumables with a thicker nickel sheath and larger crimp overlap have a smaller internal volume, decreasing the volume of tungsten carbide carried by the wire. As a result, only wires with a thin sheath and small crimp overlap (wires C, D and G in Fig. 24) contain sufficiently high tungsten carbide volume fractions to meet the typical specifications of 45–50 vol% carbide in the welded overlay. Most consumables with a thicker sheath have 35 vol% or less tungsten carbide prior to welding. Current commercial consumables use angular eutectoid W_2C/WC carbides with a size range of 30–160 μm although mono-crystalline WC is also available.

Welding with Ni–WC wires can be accomplished using standard GMAW power supplies operating in CV mode with commercially available shielding gas blends. Feeding of the stiff and kink-prone Ni–WC wire is difficult and requires short welding gun cable lengths to reduce feeding resistance. Knurled drive rollers must be used with light pressure to avoid crushing the wires during feeding. Manual welding operation is possible with either a stringer bead technique or a slight weave perpendicular to the travel direction. Typical deposition rates can range from 4.4 lb/h (2.0 kg/h) to 14.8 lb/h (6.7 kg/h) depending on the consumable. HI management with the Ni–WC material system is crucial to avoiding dissolving of the temperature sensitive tungsten carbides [67–71].

Metal transfer and HI optimization through synergic power supply waveform manipulation is not yet commercially available for

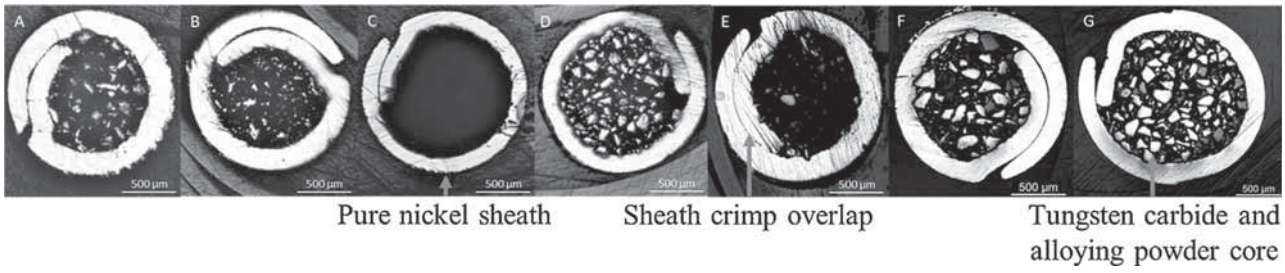

Fig. 24. Tubular Ni–WC wire cross sections showing large variability in sheath thickness and internal powder carrying volume. Wires A–F are 1/16″ (1.6 mm) diameter while G is 5/64″ (2.0 mm).

Ni–WC wires. This creates a lack of available off-the-shelf solutions for producing high tungsten carbide volume fraction overlays with tubular wires. However, hot-wire assist technology, commonly used in narrow gap groove welding or depositing corrosion resistant overlays has the potential to provide an off-the-shelf tubular wire solution. Hot-wire technology utilizes resistance joule I^2R heating to preheat the wire near its melting point without creating an arc at the electrode tip [72–76]. Formation of an arc is prevented by passing sufficiently low voltages so as to not overcome the anode and cathode fall voltages of a sustainable arc. The preheated filler material reduces the leading arc energy needed for electrode melting and base plate fusion; in turn creating a colder weld pool and reducing tungsten carbide dissolution. Hot-wire technology is typically paired with the GTAW process as the leading heat source to provide fusion with the base plate. The hot-wire GTAW process utilizing tubular Ni–WC consumables is not industrially feasible as the tungsten electrode becomes rapidly contaminated. The contamination significantly decreases arc stability and lowers productivity as the electrode has to be continually re-ground. The use of solid wires (ex. stainless steel, nickel based superalloys) does not contaminate the GTAW electrode. The hot-wire process when paired with GMAW using Ni–WC wires for both the GMAW and the hot wire is an industrially viable process. Typical deposition rates using the hot-wire GMAW process can range from 10 lb/h (4.5 kg/h) to 25 lb/h (11.4 kg/h) or higher depending on consumable selection.

In addition to the standard safety considerations when using arc welding processes, special attention must be given to fume extraction. The International Agency for Research on Cancer (IARC) lists nickel and nickel fumes as Group 1 and Group 2B materials, considered carcinogenic.

6.2. Typical materials systems

The GMAW and hot-wire processes are limited to the alloys available in wire form. Typical overlay alloys include stainless steels, nickel alloys, CCO, and nickel tungsten carbide overlays. Traditionally, stainless steel and nickel alloy overlays have been deposited with hot-wire assisted GTAW. The preheated wire decreases the arc current and weld penetration, maintaining the corrosion resistant properties of the overlay. The development of inverter GMAW power supplies with advanced waveform manipulation has allowed GMAW to clad corrosion resistant overlays with low dilution [77,78].

Wear resistant overlays typically have less stringent requirements on the maximum acceptable amount of weld dilution. CCOs are commonly deposited with the GMAW process when small volumes or small parts (e.g. pipe I.D.) require protection against service conditions. Dilution should be limited when possible as it can produce a change from a hypereutectic to hypoeutectic chemistry balance, forming lower fractions of hard M_7C_3 carbides. CCO materials form the bulk of hardfacing completed with GMAW. FCAW is another common method used to produce CCOs, making out-of-position overlays and repairs possible. There are an abundant number of commercially available wires available through many of the most common electrode producers such as Hobart, Stoody, and Lincoln. Deposition rates vary widely based on the size of wire but as an example, a 1.6 mm wire will lead to a deposition rate of ~6 to 8 lb/h [27,42,44,79]. An advantage of FCAW is that it can be used to weld down to 3″ diameter pipes [80].

The use of tubular Ni–WC wires with GMAW has traditionally resulted in poor tungsten carbide volume fractions [67–70]. Recent understanding of the carbide loss mechanisms as well as the use of hot-wire assist technology can make the GMAW process viable for industrial scale production.

6.3. Typical applications

Energy, mining, and construction industries rely heavily on equipment protection for improving in-service life cycles. In Canada, oil sands ground engaging equipment and downhole drilling tools for SAG-D wells operate in severe environments containing corrosion fluids and highly erosive sand particles. This leads to high wear rates and increased equipment down time. Ni–WC overlays have been deemed the current material system of choice to combat the severe operating conditions found in energy extraction in Alberta, Canada. While Ni–WC material systems are mainly used for severe operating conditions in oil sands mining, downhole drilling tools are exclusively protected with Ni–WC for maximum wear resistance.

Tubular Ni–WC consumables are likely to see increased usage in the near future. Research currently underway at the CCWJ with hot-wire GMAW shows promise with low dilution, high tungsten carbide volume fractions, and no detrimental carbide dissolution. The welding power supplies used in GMAW and hot-wire GMAW are small fractions of the capital expenditures required for PTAW or laser cladding systems. This low cost alternative can allow small and medium-sized fabricators to produce high value-added Ni–WC overlays. The relatively small size of the GMAW and hot-wire GMAW torches enables the process to be used for small bore I.D. cladding where the larger heads of PTAW and laser processes cannot access small features.

Another common use of GMAW-related processes for welding overlays is for internal CCOs in pipes. For large diameters this can be done using SAW but for smaller internal diameters MCAW/FCAW is almost exclusively used.

6.4. Typical challenges

While FCAW and MCAW behave in predictable ways, the GMAW welding of Ni–WC wires presents two major challenges: excessive tungsten carbide dissolution and low carbide transfer efficiencies. Previous research using tubular Ni–WC consumables is limited [67–71]. Excessive tungsten carbide dissolution was observed to be the dominant carbide loss mechanism, leading to low carbide volume fractions and poor wear resistance.

Recent GMAW research using tubular Ni–WC wires has shown that the non-wetting behavior of tungsten carbide plays an important role in the retained tungsten carbide volume fraction in the deposit [32]. The non-wetting behavior is documented during short-circuit and free flight metal transfer modes. Tungsten carbide dissolution was observed during globular free flight transfer while it was not evident during short-circuit transfer. The GMAW Ni–WC process is very sensitive to process variations, either in weld parameter changes or torch movement inconsistencies, often resulting in undesirable overlay characteristics. This is especially true when using thin sheathed consumables as changes in technique, CTWD, or welding parameters including shielding gases can drastically change the amount of tungsten carbide retained in the weld deposit. In general, thicker nickel sheathed consumables have less sensitivity to process variations but contain lower tungsten carbide volume fractions.

6.5. Typical process parameters

GMAW overlays produced with tubular Ni–WC consumables are typically welded in CV mode in either short-circuit or globular metal transfer modes. A range of welding parameters from literature are listed in Table 5. Welding is typically completed using manual welding techniques and HI should be minimized wherever possible to reduce the amount of carbide dissolution. In general, Ni–WC wires of 5/64″ (2.0 mm) or smaller are used, however, large

Table 5
Range of previously studied welding parameters.

Wire diameter (mm)	Material system	Shielding gas	Transfer mode	CTWD (mm)	Current (A)	WFS (m/min)	Voltage (V)	Travel speed (m/min)	HI-low (kJ/mm)	HI-high (kJ/mm)	Deposition rate (kg/h)	Carbide fraction (vol%)	Reference
1.6	Ni3Cr2.2B0.2Si–W_2C/WC	97.5Ar–2.5CO_2	Globular[a]	20–22	77–258	1.9–7.0	–	–	0.22–0.26	2.09–2.34	2.1–7.8	–	[67]
1.6	Ni3Cr1.5B2.5Si – W_2C/WC	97.5Ar–2.5CO_2	Globular[a]	20–22	100–247	1.2–5.3	–	–	0.22–0.28	1.26–1.54	1.4–6.3	–	[67]
1.6	Ni3Cr2.5B1Si–W_2C/WC	97.5Ar–2.5CO_2	–	–	70–170	1.1–3.3	12.8–16.2	–	–	–	–	23.3–45.2	[69]
1.6	NiB–W_2C/WC	98Ar–2O_2	SC	19	206–380	3	15.6–17.2	0.27–0.30	0.43	0.57	–	45–49[b]	[70]
1.6	NiB–W_2C/WC	98Ar–2O_2	Globular/spray	19	173–298	6.3	20.2–31.9	0.30–0.49	0.53	1.12	–	15–40[c]	[70]

[a] Stated as a program (Pr. 39) of Castolin power supply.
[b] Higher vol% of carbide in overlay than the welding wire (55 wt% carbide which is ~40 vol%).
[c] Higher vol% of carbide in overlay than the welding wire (50 vol% carbide is claimed in reference [70] but was measured to be 35 vol% at CCWJ).

diameters can also be utilized. Welding can be completed with hard automation or robotics for large surface area cladding however torch cable lengths should be kept to a minimum to avoid feeding issues. Manufacturer recommended welding parameters and shielding gases should be used as a reference wherever possible. It should be noted that production of the highest tungsten carbide volume fraction overlays may require modification to the recommended parameters and internal company and application specific welding optimization studies should be conducted. When optimizing Ni–WC overlays, traditional measures of a "good" weld should not be used. Bead appearance, high number stress-relief cross checks, and good metal transfer "sound" (especially during short-circuit) should be disregarded while the tungsten carbide volume fraction in the deposited weld should be used as the overlay quality metric. Measurement of the tungsten carbide volume fraction should be conducted on the entire weld bead for a representative sample; measurement of the volume fraction on small regions of the weld may be misleading because of inhomogeneities in the deposits.

The typical operating ranges for FCAW CCOs vary widely from 0.9 to 3.2 mm diameter, 22 to 38 V, 160 to 520 A, 300 to 800 mm/min [21,29,35,44,79].

6.6. Typical microstructures

The effect of chromium is magnified in Ni–WC GMAW as the hotter weld pool creates increased dissolution and re-precipitation of inferior secondary phases at lower chromium concentrations than equivalent PTAW overlays, shown in Fig. 25 [67,68].

The carbide volume fraction of a typical 1/16″ (1.6 mm) diameter GMAW wire is shown in Fig. 26. For comparison, a hot-wire GMAW weld completed with two 1/16″ (1.6 mm) diameter wires and higher carbide volume fraction is also shown for reference. To extend equipment lifetime, thick Ni–WC deposits are often required. A multi-pass 2-layer hot-wire GMAW overlay is shown in Fig. 27 with near uniform carbide volume fraction distribution throughout the thickness. Uniform carbide distributions will provide consistent wear rates over the overlay lifetime compared to segregated overlays.

7. Oxy-acetylene flame brazing

7.1. Description of process

Oxy-acetylene flame brazing, although being one of the oldest hardfacing technologies [81], is still popular because of its simple operation. The equipment is relatively inexpensive which includes a torch, oxygen and acetylene gas cylinders, two pressure regulators, and gas hoses for connection. The oxygen and acetylene gases at specific pressure are fed through two different pipes which mix in the torch and create a flame at the tip. Temperatures up to 3500 °C can be attained at the inner core of the oxy-acetylene flame [82]. The flame is used to locally heat but not melt the base metal before brazing; in steels, the surface acquires a glazed appearance (also called "sweating") which is an indication of the appropriate temperature to start brazing [83]. A low melting temperature hardfacing filler material is then introduced into the flame which flows onto the underlying surface and forms an overlay [84]. Brazing is typically a manual process, and there are no records of it having ever been automated. A schematic of the process as it is used for overlays is shown below in Fig. 28.

Flame brazing can be used for hardfacing most ferrous and nonferrous materials, the common ones being steel and cast iron parts due to their wide scope of applications. The surface preparation is critical to ensure there is a good bonding between the base

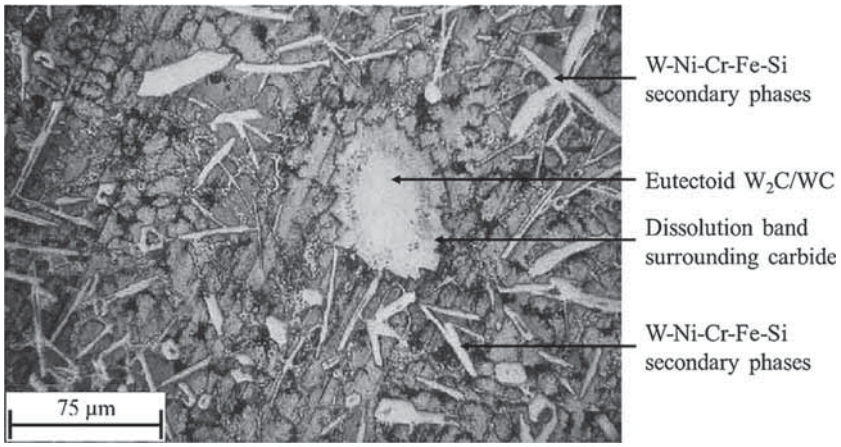

Fig. 25. GMAW overlay with matrix containing 3 wt% chromium and high fractions of re-precipitated W–Ni–Cr–Fe–Si secondary phases [67].

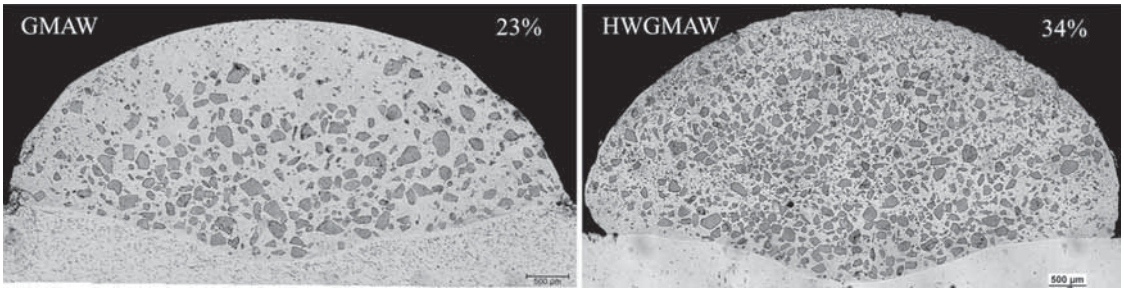

Fig. 26. Comparison of short-circuit GMAW and hot-wire assist GMAW overlays. Indicated carbide volume fractions are total weld measurements representative of the overlay wear performance.

substrate and the coating. For the metals that are not reactive, grit blasting or even solvent degreasing might be sufficient before hardfacing [85]. However, the materials that actively oxidize under heat (high chromium steels) or do not readily wet the brazing alloy are required to be coated with protective flux or a thin layer of metal alloy before brazing [84,85]. In most steels, a thin layer of self-fluxing metal alloy is thermally sprayed onto the surface that has metallurgical compatibility with the hardfacing material. During brazing, the thin flux coating melts and mixes with the hardfacing to form a strong bond with the base steel.

Rods and flexible cords are the general form of consumables used in oxy-acetylene brazing; cord is preferred because of its continuous feeding capability. The flexible cord consists of a thin metal alloy wire in its core and the cord is extruded to the required diameter by powdered alloys mixed in an organic plasticizer for binding strength [86,87].

The benefits of using flame for hardfacing are realized when low process temperatures, no base metal dilution, flexibility for hardfacing around complex geometry, and low cost, portable equipment are required [88].

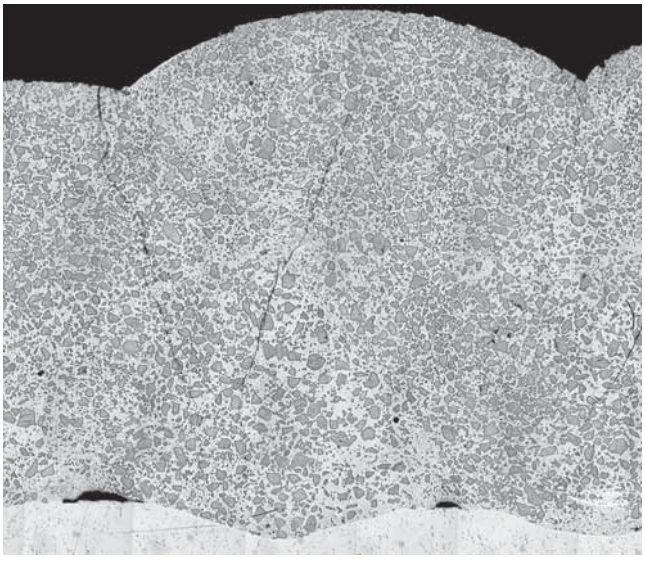

Fig. 27. Hot-wire GMAW multi-pass 2-layer deposit showing uniform carbide distribution. Deposit is approximately 7 mm thick.

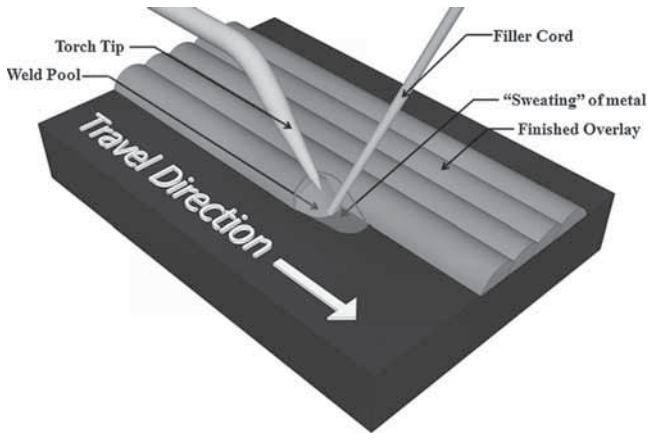

Fig. 28. Schematic of the brazing process used for depositing wear resistant overlays.

The required PPE includes shaded goggles and/or face mask (shade value of 5) to protect the eyes from infrared and ultraviolet rays present in the flame and also from flying hot particles, welding gloves to protect the hands from radiant heat and flame retardant jacket. For protection from fumes, the welding area needs to have an exhaust system. An additional fume respirator is recommended for people with respiratory concerns.

7.2. Typical materials systems

Most wear resistant materials that are used in arc welding, plasma, or laser based systems can also be used with the flame brazing process. Iron based flexible rods or cords are available that are alloyed in low or high concentrations of other components, usually chromium, molybdenum, manganese, nickel, cobalt, etc. CCOs are particularly used to get high abrasion and moderate impact resistance properties in the overlays. Nickel and cobalt based alloy systems are used to provide corrosion resistant and low friction coefficient coatings; Stellite (cobalt–chromium–tungsten) rods are more common in this category. Several varieties of tungsten carbide powders, such as cast and crushed, spherical cast, sintered, and mono-crystalline, in conjunction with nickel, cobalt, or iron based matrix systems are widely used in high stress abrasion, impact, and erosion wear environments [86,87,89]. NiCrBSi based matrices are more common with tungsten carbide systems because of their high abrasion resistance, self-fluxing, and low melting alloy characteristics [86].

The flame brazing process is often preferred to deposit tungsten carbide based material systems because the low temperatures during the process can decrease carbide dissolution. In addition, a wide range of tungsten carbide particle sizes from 100 to 2500 μm can be deposited using this process [86,87], with near 100% deposition efficiency.

7.3. Typical applications

Flame brazing is nearly universally used to deposit tungsten carbide based material systems in drill bits, and also used in stabilizer blades in petroleum industry, bucket teeth in mining industry, mixer blades, screws and conveyors in chemical and food industry, and other tools used in road construction, excavation, and dredging applications, which operate in extreme wear environments. CCOs are mainly used for hardfacing mixer blades, breakers, and hammers for concrete and mineral processing and also in agriculture earth-moving and tilling equipment that operate in high abrasion and moderate impact conditions. Stellite-based alloys are generally used to encounter abrasion, corrosion, galling, and perform at high temperatures in gas turbine vanes, blades, bushings, spacers and a range of other components.

The process is economical when low skill manual operation is preferred at fabrication shop or on-site repair and deposition rates are not critical.

7.4. Typical challenges

Having the lowest intensity heat source among other processes used for welding overlays, flame brazing comes with its own challenges. The requirement of high pre-heat (about 350 °C for alloyed steels) and high HI during the process can cause warping or distortion of the parts [88].

The low intensity of the oxy-acetylene heat source means low deposition which lowers the time efficiency of the process. The energy efficiency of the process is also low compared to other overlaying techniques as it requires high pre-heat and high HI.

The flame from an oxy-acetylene torch being so wide combined with its high HI characteristics contribute in creating a bigger and highly fluid molten pool that is difficult to control; hence, it is challenging to automate such a process. In manual operation, precise control of coating thickness is difficult, leading to excess use of materials and additional resources for grinding. Having a larger flame also makes using thinner cords not a viable option and hence limiting the smallest bead possible; this limits the process being used in certain repair jobs.

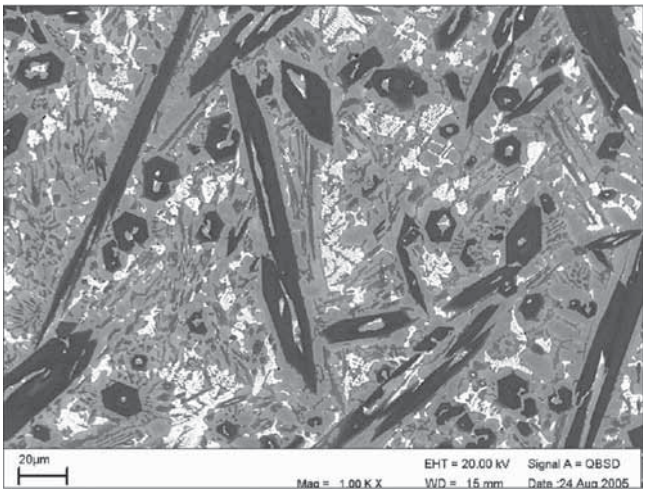

Fig. 29. Scanning electron micrograph of Stellite 190 deposited by oxy-acetylene brazing [90].

Flame brazing is not considered as the best option for working with thick sections [88]. Thick parts offer a larger heat sink which diffuses heat faster from the working area, making it difficult to braze.

In flame brazing, the bond strength of the overlay with the base metal is not as high as other fusion welding processes.

7.5. Typical process parameters

The three most important parameters in flame brazing are choosing appropriate torch tip, adjusting the pressure individually in the oxygen and acetylene tank, and selecting suitable cord type and size for the application. The torch tips are classified into different size numbers according to their tip opening diameters; the higher size number refers to a wider opening which implies higher flow rate of the gases and higher power output. The oxygen and acetylene pressure is dependent on the torch design and should be adjusted according to the supplier specification. For example, Technogenia™ recommends using 0.8–1 bar for acetylene and 4–5 bars for oxygen in their torches. The cord type and size is selected based on the requirements of performance and deposition rate for a specific application. The selection of the cord size also influences the choice of the tip size. For example, using 8 mm thick cord for high deposition rate would require higher power from the torch and warrant using a 2.6 mm diameter or wider tip opening.

The oxy-acetylene flame can be neutral, reducing, or oxidizing depending on the oxygen and acetylene proportions in the flame. A slightly carburizing or reducing flame, which is produced when the acetylene proportion is higher than stoichiometric, is preferred while hardfacing to prevent oxidation issues [83]. The flame can

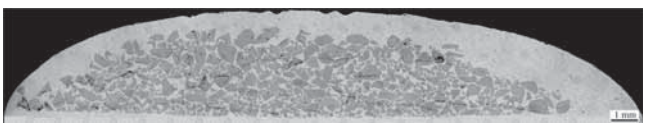

Fig. 30. Cross section of a two layer oxy-acetylene flame brazing overlay.

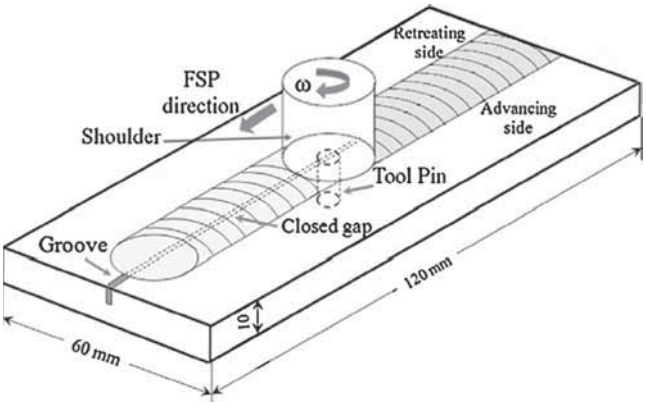

Fig. 31. Schematic of composite fabrication process by FSP [95].

be made acetylene rich by controlling the flow rate of individual gases through the needle valves present on the torch handle. Typical deposition rates are of the order of 2.2 lb/h [88], and there are unconfirmed claims of up to 6 lb/h.

7.6. Typical microstructures

Fig. 29 illustrates a typical Stellite deposition by oxy-acetylene brazing process. The Stellite alloy in the micrograph is composed of cobalt, chromium, tungsten and traces of iron, carbon and other elements. The long dark rod-like phases seen in the micrograph are chrome-rich primary carbides that provide the high abrasion resistance to the overlay. The smaller dark polygons are also the primary carbides aligned in different planes. The small grey particles dispersed across the photo are the secondary (Cr, W)C and the white patches are tungsten rich carbides, all of which are bound in a light grey CoCr alloy matrix [90].

Fig. 30 shows a brazed overlay of cast and crushed tungsten carbide in nickel alloy matrix deposited on top of steel. The volume fraction of carbides in the overlay is measured as 46 vol% which is nearly 100% of the volume fraction of carbide contained in the filler cord. This and similar observations confirm ~100% deposition efficiency, much better than other Ni–WC overlay processes. It is also to be noted that high weld pool temperatures and long cooling times, characteristic of brazing, can lead to excessive detrimental carbide dissolution. Varying levels of carbide dissolution are typically observed with the brazing process.

8. Friction stir processing

8.1. Description of process

FSP is a relatively new metalworking technique based on FSW developed in 1991 by The Welding Institute (TWI) [91]. In FSW a non-consumable rotating tool, with certain geometry, traverses along the weld line; the high rotating speed of the tool along with the frictional forces between the work piece and the shoulder promote joining by frictional heating, softening and severe plastic deformation [92]. FSP involves the same principles as FSW, but rather than joining two pieces it is used for microstructural modification, homogenization of powder metallurgy and cast parts and fabrication of metal matrix composite layers on different metallic substrates [93]. During FSP, the stirring action of the rotating tool mixes the stir zone material and this feature has been used for production of metal matrix composites [93,94]. As shown in Fig. 31, for composite fabrication by FSP, first a groove or a number of holes are machined on the surface of the matrix metal and the reinforcement is inserted into the groove/holes; then single or multi-pass FSP is performed along the groove. Material flow induced by the pin mixes the two materials and a composite layer is achieved. It should be noted that a remarkable feature of FSW/FSP is that no bulk melting occurs during the process [92], therefore deterioration of mechanical properties or dissolution of the reinforcing material, which are typical in fusion welding techniques, are limited.

8.2. Typical materials systems

This technique has been utilized for fabrication of aluminum matrix composites [95–110], magnesium matrix composites [111–117], copper matrix composites [118,119], and steel matrix composites [120,121]. FSP is typically applied to lower melting temperature alloys, as tool wear becomes a major issue for higher melting temperature systems such as ferrous alloys [122].

FSP has also been utilized as a secondary process for homogenization of composites produced by other techniques. Morisada et al. have thermally sprayed a layer of WC–CrC–Ni on a SKD61 steel substrate and then modified the composite overlay by FSP [123]. Their results show that FSP eliminates the defects in the WC–CrC–Ni layer and refines the Ni binder and the Cr_3C_2 particles. Zahmatkesh and Enayati produced a layer of Al–10%Al_2O_3 on Al 2024 substrate by using air plasma spray and then applied FSP to improve the distribution of alumina particles. They achieved a surface composite layer of 600 μm thickness with this method [124]. In a recent study, Hodder et al. applied FSP to a surface composite layer of Al–Al_2O_3 which was produced by cold gas dynamic spraying at low pressure. The redistribution of particles imposed by FSP significantly improved the mechanical properties [125].

8.3. Typical challenges

In composite fabrication using FSP, achieving uniform distribution and controlling the volume fraction of the reinforcing phase remain the main challenges. Special tool designs, applying multi-passes of FSP and multi passes with different tool geometries are the suggested techniques to improve the distribution of the reinforcement [96–98,111]. Extensive loss of the particles can occur if performing FSP directly after the particles are inserted into the groove. However this material loss can be effectively avoided by applying a single “capping” or “surface treatment” pass on the filled groove with a simple cylindrical tool that has no pin [111,112,126,127]. Some researchers have sealed the groove with a thin covering plate and then performed FSP on the plate along the groove [97,99].

Another major issue of FSW/FSP of composite materials is tool wear [97,121,128,129], which happens as a result of contact between the hard particles and the tool in conjunction with the high stresses and relatively high temperatures induced during FSP. Prado et al. have indicated extensive tool wear when FSW Al 6061–20 vol% Al_2O_3 with tool made up of carbon steel [129] as shown in Fig. 32. Considerable tool wear is also reported for a tool made up of hard WC–Co alloy during FSW of Al–Si reinforced with 30 vol% of SiC [128].

8.4. Typical process parameters

The key parameters involved with the process are tool geometry, rotation speed, travel speed and number of passes. A great deal of research work has been performed to study effects of tool features on material flow patterns during FSW/FSP[92,122,130,131]. In terms of composite fabrication by FSP, material flow in the stir zone governs the particle distribution therefore; special care should be paid to tool design to achieve uniform distribution of reinforcing particles. A square probe tool is more effective in uniformly distributing SiC particles in an aluminum matrix when compared to

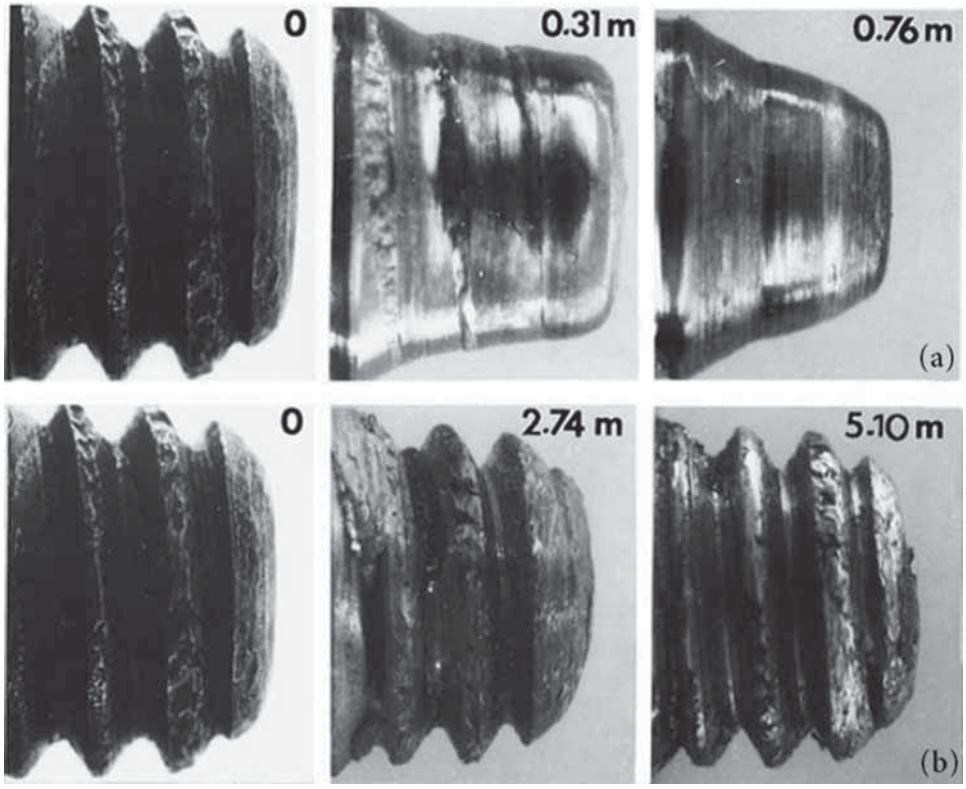

Fig. 32. Tool wear during FSW of Al 6061 reinforced with (a) 20 and (b) 0 vol% of Al_2O_3. Linear distance traveled by the tool are indicated, all welds were performed at 1000 rpm [129].

circular or triangle probe tools [97], similar results have been also reported for Al–TiB_2 composites produced by FSP [132]. Azizieh et al. have shown best Al_2O_3 distribution in AZ31 matrix can be achieved by using a tool having a circular threaded pin without flutes [111].

In a different approach, multi-pass FSP with different tools has been used to homogenize particle distribution where the first pass was performed with a simple threaded tool and the consequent passes were done using a tool which has three flat surfaces on its threaded pin [98]. The size and shape of the stir zone also directly depends on the tool size and geometry [122].

Tool rotation determines the stirring and mixing of the stir zone material [122] therefore, an increase in tool rotation speed causes more stirring and mixing which generally results in better particle distribution [111,113]. On the other hand low rotation speeds result in limited heat generation and as the material flow is affected by the HI, complete mixing needed for uniform particle distribution will not occur. Travel speed is also influential to HI and material flow; increasing the travel speed lowers the HI in a detrimental way to material flow and good particle distribution [111,113].

8.5. Typical microstructures

The microstructure of the stir zone of composites produced by FSP generally consists of a uniform distribution of the particles in a matrix with refined grains. Grain refinement happens as a result of dynamic recrystallization which takes place during FSW/FSP [122]. As discussed before, FSP is a solid state process; therefore, chemical reactions between the matrix alloy and the reinforcement, or dissolution of the reinforcement are not probable. However, dissolution of the precipitates available in the parent material may occur during FSW/FSP of heat treatable aluminum alloys [122,133]. The microstructure of the FSP produced layer is directly influenced by many factors mainly the rotation speed of the pin [125]. Fig. 33

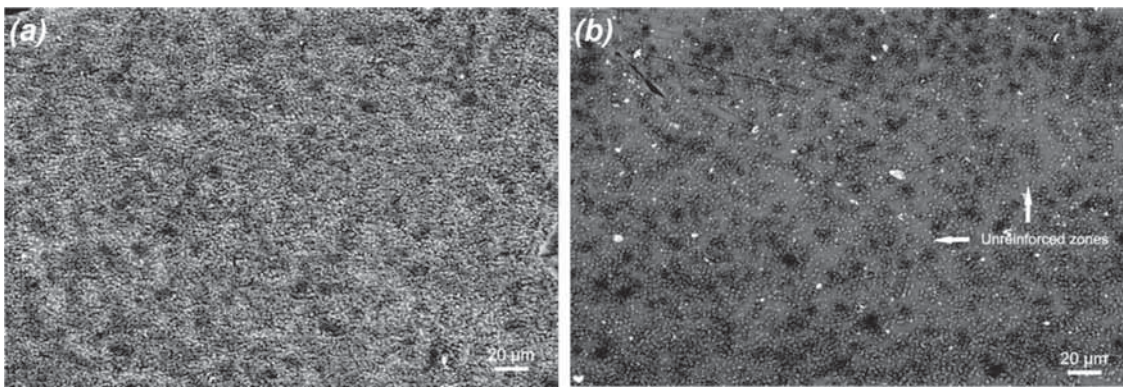

Fig. 33. SEM micrograph of cold-sprayed coating fabricated from Al–90 wt% Al_2O_3 powder blend after FSP at (a) 894 rpm and (b) 1723 rpm [125].

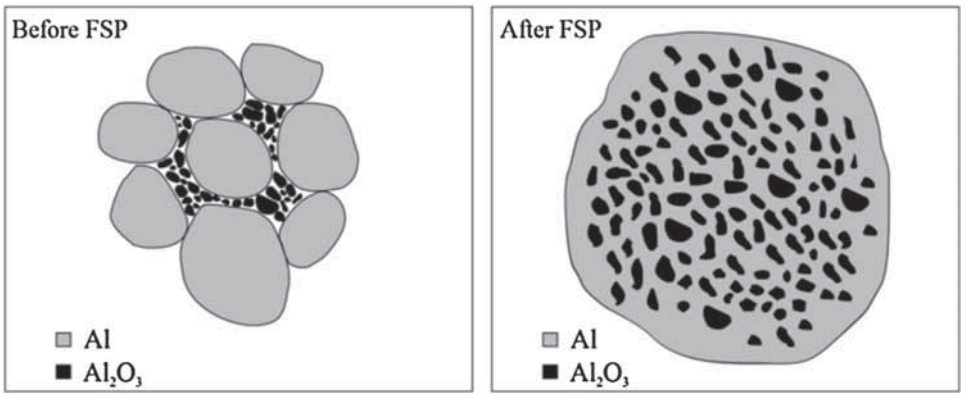

Fig. 34. Schematic of reinforcing particle re-distribution in cold-sprayed MMC coatings during FSP [125].

Table 6
Summary of wear properties and hardness values for overlays produced by different processes.

Process	Alloy system	Reinforcement fraction (vol%)	Hardness Vickers (kg)			G65 Procedure A mass loss (g)	Cost of raw material ($/kg)	Reference
			Carbide	Matrix	Overall			
PTAW	Ni	–	–	300–750 (1)	300–750 (1)	0.2–1.85	–	[7]
	Ni–WC	30–50	2200 (1)	300–750 (1)	500–900 (1)	0.04–0.098	150	[2,7]
SMAW	CCO steel	–	–	–	587–940 (1)	0.12–0.292	30–80	[21,24,26,27,29, 35,43,44,134–136]
FCAW	CCO steel	–	1050–1600 (1)	500–750 (1)	639–746 (1)	0.16–0.26	25–50	
SAW	CCO steel	30–60	–	–	543–746 (1)	0.15–0.26	30–80	
GMAW	Ni–WC	14–30	2360 (0.2)	500–600 (1)	–	0.161–0.294	150	CCWJ, [69]
Hot-Wire GMAW	Ni–WC	30–40	2200 (0.2)	770 (1)	–	0.086–0.161	150	CCWJ
Brazing	Ni–WC[a]	40–52	2500–3500 (0.1)	380–450 (0.3)	–	0.04–0.12	160–195	[Informal industry survey]
	Ni–WC[b]	40–52	2300 (0.1)	420–450 (0.1)	–	0.05–0.15	105–145	
LBW	Ni–WC	40–50	2700–3400 (0.1)	400–560 (0.1)	–	0.05–0.08	88–132	[Informal industry survey]
FSP	A 390–Al_2O_3	–	–	120 (0.06)	224 (0.06)	4.5×10^{-6}[c]	–	[137]
FSW and thermal spray	Steel-WC/CrC/Ni	–	2084 (0.3)	1500[d](0.3)	2000 (0.3)	–	–	[123]

[a] Spherical tungsten carbide reinforcement.
[b] Angular tungsten carbide reinforcement.
[c] ASTM G99-95 test results in g/s units.
[d] Hardness of the as-sprayed carbide layer prior to FSW.

shows the microstructure of a cold-sprayed overlay after FSP at different rotation speeds.

A schematic representation of the breakdown and redistribution of the reinforcing particles during FSP in a cold-sprayed overlay is displayed in Fig. 34.

9. Summary

This paper reviewed the most popular materials and processes for the weld deposition of wear resistant overlays. The most popular materials systems are Ni–WC and CCOs. These material systems occupy ends of the spectrum in characteristics.

Ni–WC can be 10–15 times more expensive than CCOs, but CCOs have a market 20 times larger. The wear performance of Ni–WC is far superior to CCOs. The challenges in deposition of these materials systems determine the type of process used. Ni–WC requires that the carbides are introduced as a second phase in the melt, and one of the main challenges is dissolution of the carbides in the molten metal. To avoid dissolution, the leading processes for Ni–WC are PTAW and LBW because of the low overheating of the weld pool. Wire-based processes present the challenge of carbides bouncing off the free-surface of the melt, resulting in very low efficiency in carbide entrapment.

In CCOs, the carbides are formed during solidification hence, overheating does not have detrimental effects similar to Ni–WC overlays. For CCOs, the leading processes are SAW for plate and MCAW (often called FCAW) for internal pipe cladding. At the typical cooling rates of CCOs, cooling rate seems to be a secondary parameter for microstructural development [32].

FSW techniques are still in their infancy, but show the promise of enabling wear properties until now impossible, especially in aluminum alloys. In addition to the reinforcement, the microstructural refinement plays a key role.

Table 6 summarizes some microstructural, hardness, and performance properties of the alloy and process combinations described above. Cost is also included, although this is a very tentative estimate.

Acknowledgments

The authors wish to acknowledge the many industrial partners of the CCWJ for sharing their knowledge and having provided material support, in particular to NSERC, Syncrude, Hitachi Canada for project funding, Wilkinson Steel and Apollo Clad for access to photos, Guy Gibbs for sharing his input and advice, and Arctec, HCStark, Lincoln, Miller, and Praxair for equipment and consumables. The authors gratefully acknowledge Dr. Adrian Gerlich for his invaluable assistance on FSP.

References

[1] Associate Committee on Tribology. National Research Council of Canada; 1987.
[2] Wolfe T. Homogeneity of metal matrix composites deposited by plasma transferred arc welding. PhD thesis. University of Alberta; 2010.
[3] Amado J, Tobar M, Yáñez A. Laser cladding of NiCr-WC metal matrix composites: dependence on the matrix composition. In: Proceedings of the 36th International MATADOR Conference. 2010. p. 459–62.
[4] Amado JM, Tobar MJ, Alvarez JC, Lamas J, Yáñez a. Laser cladding of tungsten carbides (Spherotene®) hardfacing alloys for the mining and mineral industry. Appl Surf Sci 2009;255:5553–6.
[5] Gerk C, Wernicke K. No Title. U.S. Patent. U.S. Patent No.: 7,451,090 B2; 2009.
[6] Gassmann R. Laser cladding with (WCW2C)/CoCrC and (WCW2C)/NiBSi composites for enhanced abrasive wear resistance. Mater Sci Technol 1996;12:691–6.
[7] Liyanage T. Microstructure and properties of Ni-alloy and Ni—WC composite overlays. MSc thesis. University of Alberta; 2010.
[8] Jones M, Waag U. The influence of carbide dissolution on the erosion–corrosion properties of cast tungsten carbide/Ni-based PTAW overlays. Wear 2011;271:1314–24.
[9] Dai Y, Tan X, Li Y, Yang J, Huang B. Influence of fabricating process on microstructure and properties of spheroidal cast tungsten carbide powder. Trans Nonferrous Met Soc China 2005;15:270–4.
[10] Unpublished industrial research. Apollo-Clad Laser Cladding, A Division of Apollo Machine and Welding Ltd. n.d.
[11] Cockeram BV. The fracture toughness and toughening mechanisms of nickel-base wear materials. Metall Mater Trans A 2002;33:33–56.
[12] Lin MC, Chang LS, Lin HC, Yang CH, Lin KM. A study of high-speed slurry erosion of NiCrBSi thermal-sprayed coating. Surf Coat Technol 2006;201:3193–8.
[13] Shieh Y-H, Wang J-T, Shih HC, Wu S-T. Alloying and post-heat-treatment of thermal-sprayed coatings of self-fluxing alloys. Surf Coat Technol 1993;58:73–7.
[14] Balu P, Hamid S, Kovacevic R. Finite element modeling of heat transfer in single and multilayered deposits of Ni—WC produced by the laser-based powder deposition process. Int J Adv Manuf Technol 2013.
[15] Liyanage T, Fisher G, Gerlich aP. Microstructures and abrasive wear performance of PTAW deposited Ni–WC overlays using different Ni-alloy chemistries. Wear 2012;274–275:345–54.
[16] Atamert S, Bhadeshia H. Microstructure and stability of Fe—Cr—C hardfacing alloys. Mater Sci Eng: A 1990;130:101–11.
[17] Fisher G, Wolfe T, Yarmuch M. The use of protective weld overlays in oil sands mining. Aust Weld J 2012:57.
[18] Lin C-M, Lai H-H, Kuo J-C, Wu W. Effect of carbon content on solidification behaviors and morphological characteristics of the constituent phases in Cr—Fe—C alloys. Mater Charact 2011;62:1124–33.
[19] Pearce J. Structure and wear performance of abrasion resistant chromium white cast irons. AFS Trans 1984;92:599–622.
[20] Tabrett CP, Sare IR, Ghomashchi MR. Microstructure-property relationships in high chromium white iron alloys. Int Mater Rev 1996;41:59–82.
[21] Mennon R, Wallin J, Barnhart T. The development of corrosion–abrasion resistant overlays for oil sands applications n.d.
[22] Azimi G, Shamanian M. Effects of silicon content on the microstructure and corrosion behavior of Fe–Cr–C hardfacing alloys. J Alloys Compd 2010;505:598–603.
[23] Doğan Ö, Hawk JIIGL. Solidification structure and abrasion resistance of high chromium white irons. Metall Mater Trans 1997:28.
[24] Flores JF, Neville a, Kapur N, Gnanavelu a. Erosion–corrosion degradation mechanisms of Fe–Cr–C and WC–Fe–Cr–C PTA overlays in concentrated slurries. Wear 2009;267:1811–20.
[25] Sabet H, Khierandish S, Mirdamadi S, Goodarzi M. The microstructure and abrasive wear resistance of Fe–Cr–C hardfacing alloys with the composition of hypoeutectic, eutectic, and hypereutectic at $$ \frac{Cr}{C} = 6 $$. Tribol Lett 2011;44:237–45.
[26] Buchely MF, Gutierrez JC, León LM, Toro A. The effect of microstructure on abrasive wear of hardfacing alloys. Wear 2005;259:52–61.
[27] Kotecki D, Ogborn J. Abrasion resistance of iron-based hardfacing alloys. Weld J 1995;74:269–78.
[28] Wang ZH, Wang QB, Cui L, Yang a, He DDY. Influence of cooling rate and composition on orientation of primary carbides of Fe–Cr–C hardfacing alloys. Sci Technol Weld Join 2008;13:656–62.
[29] Zhou YF, Yang YL, Jiang YW, Yang J, Ren XJ, Yang QX. Fe–24 wt.%Cr–4.1 wt.%C hardfacing alloy: microstructure and carbide refinement mechanisms with ceria additive. Mater Charact 2012;72:77–86.
[30] Turnbull D. Phase changes. Solid State Phys 1956;3:225–306.
[31] Chang C-M, Chen L-H, Lin C-M, Chen J-H, Fan C-M, Wu W. Microstructure and wear characteristics of hypereutectic Fe–Cr–C cladding with various carbon contents. Surf Coat Technol 2010;205:245–50.
[32] Mendez P. Modern technologies for the deposition of wear-resistant overlays. In: Weld overlay for wear protection. Edmonton: Canadian Welding Association; 2013.
[33] Berns H, Fischer A. Abrasive wear resistance and microstructure of Fe–Cr–CB hard surfacing weld deposits. Wear 1986;112:163–80.
[34] Liu HY, Yu FB, Meng QS, Chen SP, Wang H. Microstructure and properties of Fe–Cr–C hardfacing alloys reinforced with TiC-TiB^2. Sci Technol Weld Join 2012;17:419–23.
[35] Wang Q, Li X. Effects of Nb, V, and W on microstructure and abrasion resistance of Fe–Cr–C hardfacing alloys. Weld J 2010;89:133–9.
[36] Chotěborský R, Hrabě P, Müller M, Válek R, Savková J, Jirka M. Effect of carbide size in hardfacing on abrasive wear. Res Agric Eng 2009;55:149–58.
[37] Buchanan VE, Shipway PH, McCartney DG. Microstructure and abrasive wear behaviour of shielded metal arc welding hardfacings used in the sugarcane industry. Wear 2007;263:99–110.
[38] Buchanan VE. Solidification and microstructural characterisation of iron–chromium based hardfaced coatings deposited by SMAW and electric arc spraying. Surf Coat Technol 2009;203:3638–46.
[39] Lin C-M, Chang C -M, Chen J -H, Hsieh C -C, Wu W. Microstructure and wear characteristics of high-carbon Cr-based alloy claddings formed by gas tungsten arc welding (GTAW). Surf Coat Technol 2010;205:2590–6.
[40] Chang C-M, Chen Y-C, Wu W. Microstructural and abrasive characteristics of high carbon Fe–Cr–C hardfacing alloy. Tribol Int 2010;43:929–34.
[41] Yarmuch M. Effect of welding parameters on the plasma transferred arc welding (PTAW) process for autogenous beads and 410SS-WC overlays. MSc thesis. University of Alberta; 2006.
[42] Kirchgaßner M, Badisch E, Franek F. Behaviour of iron-based hardfacing alloys under abrasion and impact. Wear 2008;265:772–9.
[43] Flores J, Neville A. Materials selection in the oilsands industry based on materials degradation mechanisms. Explor Prod Oil Gas Rev 2009;7:42–5.
[44] Klimpel A, Dobrzański LA, Janicki D, Lisiecki A. Abrasion resistance of GMA metal cored wires surfaced deposits. J Mater Process Technol 2005;164–165:1056–61.
[45] De Oliveira U, Ocelík V, De Hosson JTM. Analysis of coaxial laser cladding processing conditions. Surf Coat Technol 2005;197:127–36.
[46] Verwimp J, Rombouts M, Geerinckx E, Motmans F. Applications of laser cladded WC-based wear resistant coatings. Phy Proc 2011;12:330–7.
[47] Lin WC, Chen C. Characteristics of thin surface layers of cobalt-based alloys deposited by laser cladding. Surf Coat Technol 2006;200:4557–63.
[48] Zhou S, Dai X, Zeng X. Effects of processing parameters on structure of Ni-based WC composite coatings during laser induction hybrid rapid cladding. Appl Surf Sci 2009;255:8494–500.
[49] Babu SS, Kelly SM, Murugananth M, Martukanitz RP. Reactive gas shielding during laser surface alloying for production of hard coatings. Surf Coat Technol 2006;200:2663–71.
[50] Chiang K, Chen aYC. Microstructural characterization and microscopy analysis of laser cladding Stellite12 and tungsten carbide. J Mater Process Technol 2007;182:297–302.
[51] Cao X, Xiao M, Jahazi M, Fournier J, Alain M. Optimization of processing parameters during laser cladding of ZE41A-T5 magnesium alloy castings using taguchi method. Mater Manuf Process 2008;23:413–8.
[52] Beyer E. New industrial systems & concepts for highest laser cladding efficiency; 2011 http://www.lia.org/blog/2011/05/high-performance-laser-cladding.
[53] CSA. CAN/CSA-E60825-1-03 (R2012) - Safety of Laser Products - Part 1: Equipment Classification, Requirements and User's Guide 2003:130.
[54] CSA. Z94.3-07 (R2012) – Eye and face protectors; 2007:86.
[55] Toyserkani E, Khajepour A, Corbin S. Laser cladding. CRC Press; 2004.
[56] Wu P, Du HM, Chen XL, Li ZQ, Bai HL, Jiang EY. Influence of WC particle behavior on the wear resistance properties of Ni–WC composite coatings. Wear 2004;257:142–7.
[57] Navas C, Cadenas M, Cuetos JM, De Damborenea J. Microstructure and sliding wear behaviour of Tribaloy T-800 coatings deposited by laser cladding. Wear 2006;260:838–46.
[58] Przybyłowicz J, Kusiński J. Structure of laser cladded tungsten carbide composite coatings. J Mater Process Technol 2001;109:154–60.
[59] Xu G, Kutsuna M, Liu Z, Sun L. Characteristic behaviours of clad layer by a multi-layer laser cladding with powder mixture of Stellite-6 and tungsten carbide. Surf Coat Technol 2006;201:3385–92.
[60] Masanta M, Ganesh P, Kaul R, Nath AK, Roy Choudhury A. Development of a hard nano-structured multi-component ceramic coating by laser cladding. Mater Sci Eng: A 2009;508:134–40.
[61] Zhong M, Liu W, Zhang Y, Zhu X. Formation of WC/Ni hard alloy coating by laser cladding of W/C/Ni pure element powder blend. Int J Refract Met Hard Mater 2006;24:453–60.
[62] Riabkina-Fishman M, Rabkin E, Levin P, Frage N, Dariel MP, Weisheit A, et al. Laser produced functionally graded tungsten carbide coatings on M2 high-speed tool steel. Mater Sci Eng: A 2001;302:106–14.
[63] Pu Y, Guo B, Zhou J, Zhang S, Zhou H, Chen J. Microstructure and tribological properties of in situ synthesized TiC, TiN, and SiC reinforced Ti3Al intermetallic matrix composite coatings on pure Ti by laser cladding. Appl Surf Sci 2008;255:2697–703.
[64] Partes K. Analytical model of the catchment efficiency in high speed laser cladding. Surf Coat Technol 2009;204:366–71.
[65] Lin J. A simple model of powder catchment in coaxial laser cladding. Opt Laser Technol 1999;31:233–8.
[66] Nowotny S, Scharek S, Kempe F, Beyer E. COAXn: Modular system of powder nozzles for laser beam build-up welding. Int Cong Appl Lasers Electro Opt 2003:519.
[67] Klimpel a, Dobrzański L, Lisiecki a, Janicki aD. The study of properties of Ni–WC wires surfaced deposits. J Mater Process Technol 2005;164–165:1046–55.
[68] Klimpel A, Lisiecki A. Robotized GMA surfacing of cermetal deposits. J Achiev Mater Manuf Eng 2006;18:395–8.

[69] Badisch E, Kirchgaßner M. Influence of welding parameters on microstructure and wear behaviour of a typical NiCrBSi hardfacing alloy reinforced with tungsten carbide. Surf Coat Technol 2008;202:6016–22.
[70] Choi L, Wolfe T, Yarmuch M, Gerlich A. Effect of welding parameters on tungsten carbide - metal matrix composites produced by GMAW effect of welding parameters on tungsten carbide – metal matrix composites produced by GMAW. Canadian Welding Association; 2010.
[71] Scott KM. Heat transfer and calorimetry of tubular Ni/WC wires deposited with GMAW by master of science. MSc thesis. University of Alberta; 2011.
[72] Manz A. Consumable electrode arcless electric working. U.S. Patent U.S. Patent No. 3,122,629, 1964.
[73] Yamamoto M, Shinozaki K, Myoga T, Kanazawa T, Arashin H. Development of ultra-high-speed GTA welding process using pulse-heated hot-wire. IIW Doc. XII-1927-07; 2007.
[74] Hori K, Watanabe H, Myoga T, Kusano K. Development of hot wire TIG welding methods using pulsed current to heat filler wire – research on pulse heated hot wire TIG welding processes. Weld Int 2004;18:456–68.
[75] Ueguri S, Tabata Y, Shimizu T, Mizuno T. Control of deposition rates in hot wire TIG welding. Weld Int 1987;1:736–42.
[76] Shinozaki K, Yamamoto M, Mitsuhata K, Nagashima T, Kanazawa T, Arashin H. Bead formation and wire temperature distribution during ultra-high-speed GTA welding using pulse-heated hot-wire. Weld World 2013;55:12–8.
[77] Pickin CG, Williams SW, Lunt M. Characterisation of the cold metal transfer (CMT) process and its application for low dilution cladding. J Mater Process Technol 2011;211:496–502.
[78] New fields of application for CMT n.d.
[79] Chang C-M, Hsieh C-C, Lin C-M, Chen J-H, Fan C-M, Wu W. Effect of carbon content on microstructure and corrosion behavior of hypereutectic Fe–Cr–C claddings. Mater Chem Phys 2010;123:241–6.
[80] http://www.indutechcanada.com/indulay.html, n.d.
[81] O'Brien A. Welding handbook, vol. 2, Ninth ed. American Welding Society (AWS); 2004.
[82] Kehl R. Oxy-acetylene welding practice. American Technical Society; 1918.
[83] Engle D. Hard facings. Ohio State Eng 1940;23:12–4.
[84] Jeffus L. Metal fabrication technology for agriculture. 2nd ed. Cengage Learning; 2011.
[85] Case Study. Hardfacing with cast tungsten carbide in a NiCrBSi matrix using a flexible cord consumable. Surf Eng 1987;3:25–7.
[86] Azzoni M. Directions and developments in the types of hard phases to be applied in braze deposits against abrasion. Weld Int 2009;23:706–16.
[87] Zatoka A, Vasil'eva V. Flexible cords for the application of protective coatings by the gas flame method. Chem Petrol Eng 1992;28:26–8.
[88] Gregory EN. Hardfacing. Tribol Int 1978;11:129–34.
[89] Pradeep G, Ramesh A, Prasad B. A review paper on hardfacing processes and materials. Int J Eng Sci Technol 2010;2:6507–10.
[90] www.stellite.co.uk, n.d.
[91] Thomas W, Nicholas E. Friction welding. In: U.S. Patent US patent No. 5460317. 1995.
[92] Nandan R, Debroy T, Bhadeshia H. Recent advances in friction-stir welding – process, weldment structure and properties. Prog Mater Sci 2008;53:980–1023.
[93] Ma ZY. Friction stir processing technology: a review. Metall Mater Trans A 2008;39:642–58.
[94] Mishra R, Ma Z, Charit I. Friction stir processing: a novel technique for fabrication of surface composite. Mater Sci Eng: A 2003;341:307–10.
[95] Alidokht S, Abdollah-zadeh a, Soleymani a, Assadi SH. Microstructure and tribological performance of an aluminium alloy based hybrid composite produced by friction stir processing. Mater Des 2011;32:2727–33.
[96] Shafiei-Zarghani a, Kashani-Bozorg SF, Zarei-Hanzaki a. Microstructures and mechanical properties of Al/Al_2O_3 surface nano-composite layer produced by friction stir processing. Mater Sci Eng: A 2009;500:84–91.
[97] Mahmoud ERI, Takahashi M, Shibayanagi T, Ikeuchi K. Effect of friction stir processing tool probe on fabrication of SiC particle reinforced composite on aluminium surface. Sci Technol Weld Join 2009;14:413–25.
[98] Izadi H, Gerlich AP. Distribution and stability of carbon nanotubes during multi-pass friction stir processing of carbon nanotube/aluminum composites. Carbon 2012;50:4744–9.
[99] Lim DK, Shibayanagi T, Gerlich aP. Synthesis of multi-walled CNT reinforced aluminium alloy composite via friction stir processing. Mater Sci Eng: A 2009;507:194–9.
[100] Bozorg SFK, Zarghani AS, Zarei-Hanzaki A, Rusop M, Subban RY, Kamarulzaman N, et al. Fabrication of nano-composite surface layers on aluminium employing friction stir processing technique. AIP Conf Proc 2010:447–51.
[101] Chen C-F, Kao P-W, Chang L, Ho N-J. Mechanical properties of nanometric Al_2O_3 particulate-reinforced Al-$Al_{11}Ce_3$ composites produced by friction stir processing. Mater Trans 2010;51:933–8.
[102] Hsu CJ, Chang CY, Kao PW, Ho NJ, Chang CP. Al–Al_3Ti nanocomposites produced in situ by friction stir processing. Acta Mater 2006;54:5241–9.
[103] Hsu CJ, Kao PW, Ho NJ. Ultrafine-grained Al–Al_2Cu composite produced in situ by friction stir processing. Scripta Mater 2005;53:341–5.
[104] Hsu CJ, Kao PW, Ho NJ. Intermetallic-reinforced aluminum matrix composites produced in situ by friction stir processing. Mater Lett 2007;61:1315–8.
[105] Kashani-Bozorg SF, Jazayeri K, Rusop M, Soga T. Formation of Al/B[sub 4]C surface nano-composite layers on 7075 Al alloy employing friction stir processing. AIP Conf Proc 2009:715–9.
[106] Mahmoud ERI, Ikeuchi K, Takahashi M. Fabrication of SiC particle reinforced composite on aluminium surface by friction stir processing. Sci Technol Weld Join 2008;13:607–18.
[107] Mahmoud ERI, Takahashi M, Shibayanagi T, Ikeuchi K. Fabrication of surface-hybrid-MMCs layer on aluminum plate by friction stir processing and its wear characteristics. Mater Trans 2009;50:1824–31.
[108] Mahmoud ERI, Takahashi M, Shibayanagi T, Ikeuchi K. Wear characteristics of surface-hybrid-MMCs layer fabricated on aluminum plate by friction stir processing. Wear 2010;268:1111–21.
[109] Morisada Y, Fujii H, Nagaoka T, Nogi K, Fukusumi M. Fullerene/A5083 composites fabricated by material flow during friction stir processing. Compos Part A: Appl Sci Manuf 2007;38:2097–101.
[110] Yang M, Xu C, Wu C, Lin K, Chao YJ, An L. Fabrication of AA6061/Al_2O_3 nano ceramic particle reinforced composite coating by using friction stir processing. J Mater Sci 2010;45:4431–8.
[111] Azizieh M, Kokabi A, Abachi HP. Effect of rotational speed and probe profile on microstructure and hardness of AZ31/Al_2O_3 nanocomposites fabricated by friction stir processing. Mater Des 2011;32:2034–41.
[112] Lee C, Huang J, Hsieh P. Mg based nano-composites fabricated by friction stir processing. Scripta Mater 2006;54:1415–20.
[113] Morisada Y, Fujii H, Nagaoka T, Fukusumi M. MWCNTs/AZ31 surface composites fabricated by friction stir processing. Mater Sci Eng: A 2006;419:344–8.
[114] Asadi P, Faraji G, Besharati MK. Producing of AZ91/SiC composite by friction stir processing (FSP). Int J Adv Manuf Technol 2010;51:247–60.
[115] Chang C, Wang Y, Pei H. Microstructure and mechanical properties of nano-ZrO_2 and nano-SiO_2 particulate reinforced AZ31-Mg based composites fabricated by friction stir processing. Key Eng Mater 2007;351:114–9.
[116] Morisada Y, Fujii H, Nagaoka T, Fukusumi M. Effect of friction stir processing with SiC particles on microstructure and hardness of AZ31. Mater Sci Eng: A 2006;433:50–4.
[117] Wang K, Chang L. Preparation of Mg-AZ31 based composites with Ti particles by friction stir processing. Chin J Nonferrous Met 2009;19:418–23.
[118] Chen WL, Huang CP, Ke LM. A novel way to fabricate carbon nanotubes reinforced copper matrix composites by friction stir processing. Adv Mater Res 2011;391–392:524–9.
[119] Barmouz M, Asadi P, Besharati Givi MK, Taherishargh M. Investigation of mechanical properties of Cu/SiC composite fabricated by FSP: effect of SiC particles' size and volume fraction. Mater Sci Eng: A 2011;528:1740–9.
[120] Salekrostam R, Besharati Givi MK, Asadi P, Bahemmat P. Influence of friction stir processing parameters on the fabrication of SiC/316L surface composite. Defect Diffus Forum 2010;297–301:221–6.
[121] Ghasemi-Kahrizsangi A, Kashani-Bozorg SF. Microstructure and mechanical properties of steel/TiC nano-composite surface layer produced by friction stir processing. Surf Coat Technol 2012;209:15–22.
[122] Mishra RS, Ma ZY. Friction stir welding and processing. Mater Sci Eng: R: Rep 2005;50:1–78.
[123] Morisada Y, Fujii H, Mizuno T, Abe G, Nagaoka T, Fukusumi M. Modification of thermally sprayed cemented carbide layer by friction stir processing. Surf Coat Technol 2010;204:2459–64.
[124] Zahmatkesh B, Enayati MH. A novel approach for development of surface nanocomposite by friction stir processing. Mater Sci Eng: A 2010;527:6734–40.
[125] Hodder KJ, Izadi H, McDonald a, Gerlich GPa. Fabrication of aluminum–alumina metal matrix composites via cold gas dynamic spraying at low pressure followed by friction stir processing. Mater Sci Eng: A 2012;556:114–21.
[126] Devaraju a, Kumar a, Kotiveerachari B. Influence of rotational speed and reinforcements on wear and mechanical properties of aluminum hybrid composites via friction stir processing. Mater Des 2013;45:576–85.
[127] Soleymani S, Abdollah-zadeh A, Alidokht Sa. Microstructural and tribological properties of Al5083 based surface hybrid composite produced by friction stir processing. Wear 2012;278-279:41–7.
[128] Liu HJ, Feng JC, Fujii H, Nogi K. Wear characteristics of a WC–Co tool in friction stir welding of AC4A + 30 vol%SiCp composite. Int J Mach Tools Manuf 2005;45:1635–9.
[129] Prado R, Murr L. Tool wear in the friction-stir welding of aluminum alloy 6061 + 20% Al_2O_3: a preliminary study. Scripta Mater 2001;45:75–80.
[130] Elangovan K, Balasubramanian V, Valliappan M. Effect of tool pin profile and tool rotational speed on mechanical properties of friction stir welded AA6061 aluminium alloy. Mater Manuf Process 2008;23:251–60.
[131] Rai R, De a, Bhadeshia HKDH, DebRoy T. Review: friction stir welding tools. Sci Technol Weld Join 2011;16:325–42.
[132] Vijay SJ, Murugan N. Influence of tool pin profile on the metallurgical and mechanical properties of friction stir welded Al–10 wt.% TiB2 metal matrix composite. Mater Des 2010;31:3585–9.
[133] Threadgill PL, Leonard a J, Shercliff HR, Withers PJ. Friction stir welding of aluminium alloys. Int Mater Rev 2009;54:49–93.
[134] Buytoz S. Microstructural properties of M7C3 eutectic carbides in a Fe–Cr–C alloy. Mater Lett 2006;60:605–8.
[135] Liu ZJ, Su YH, Sun JG. Effects of shape and distribution of M_7C_3 on wear resistance of iron based composite. Key Eng Mater 2008;373-374:560–3.
[136] Fisher G, E Al. The use of protective weld overlays in oil sands mining. Aust Weld J 2012;57:12.
[137] Raaft M, Mahmoud TS, Zakaria HM, Khalifa Ta. Microstructural, mechanical and wear behavior of A390/graphite and A390/Al_2O_3 surface composites fabricated using FSP. Mater Sci Eng: A 2011;528:5741–6.